ISSN: 2588-5596

JGT

Journal of Gas Technology

Volume 3 . January 2018 . www.jgt.irangi.org

Journal of Gas Technology, JGT

Volume 3. January 2018

Contact Information
Iranian Gas Institute:
http://www.jgt.irangi.org
Journal Email Address:
ijgt.igi@gmail.com

ISSN: 2588-5596

Table of Contents

Prediction of H_2S and CO_2 Solubility in Aqueous MDEA and MDEA/PZ Solutions Using ELECNRTL and ACID GAS Packages

• **Omid Sabbagh, Maissam Vahidi Ferdowsi, Mohammad Ali Fanaei***
Department of Chemical Engineering, Ferdowsi University of Mashhad, Mashhad, Iran
Corresponding author Email address: fanaei@um.ac.ir

Received: Feb. 24, 2017 / Accepted: Apr. 20, 2017

Abstract

In this study, the solubility of acid gases of hydrogen sulfide and carbon dioxide in MDEA and MDEA/PZ aqueous solutions was evaluated by different thermodynamic packages. Comparison of modeling results with a series of laboratory and industrial data released from 1997 to 2010 indicates the high accuracy of ACID GAS thermodynamic package (Aspen HYSYS 8.3) to prediction of acid gases solubility in the mentioned solutions compared to the ELECNRTL thermodynamic package (Aspen plus V8.2), especially in the range of acid gases operational concentration in the gas refineries.

Keywords: MDEA, PZ, Thermodynamic package, Acid gas solubility, Acid gas, ELECNRTL

1. INTRODUCTION

Sour gas sweetening is one of the most important natural gas refining processes, which is done to remove acid gases such as H_2S and CO_2 in order to reduce the corrosion rate, improve the gas quality, reduce the toxicity of catalysts, etc. Alkanolamines such as MDEA, DEA and mixtures of MDEA/PZ and MDEA/DEA are used as the most common chemical solvents for natural gas sweetening.

Prediction of H_2S and CO_2 solubility in amine solutions is highly essential to design and simulation of natural gas sweetening units. For this purpose, various thermodynamic packages inserted in the popular commercial softwares, such as ASPEN HYSYS and ASPEN PLUS. Two main approaches that are used in these packages are known as "Correlation-Based" and "Activity Coefficient Model-Based". "AMINE" and "APISOUR" packages are examples of the first approach, and "ELECNRTL" and "ACID GAS" packages are examples of the second approach.

Many studies have been done on predicting the solubility of acid gases in amine solutions. Deshmukh and Mather (1981) used the activity coefficients model to predict the solubility of H_2S and CO_2 in amine solutions [1]. Posey et al. (1996) used a simple correlation for prediction of acid gas solubility in alkanolamines [2]. Prashanth Patil et al. (2006) evaluated the solubility of H_2S and CO_2 in MDEA aqueous solution by the extended correlation of Kenneth Eisenberg [3]. Huttenhuis et al. (2009) investigated the Solubility of CO_2 and H_2S in aqueous MDEA solutions, experimentally [4]. Ying Zhang et al. (2011) also examined CO_2 absorption in aqueous MEA and MDEA solutions with electrolyte NRTL model [5, 6].

According to development of chemical process simulators in the last years, many of studies are focused on comparison of them together. Hansen et al. (2011) compared the ASPEN HYSYS and ASPEN PLUS softwares accuracy in predicting of CO_2 absorption by MEA solution [7]. Erik Øi (2012) did a same work but this study was focused on CO_2 removal from exhaust gas [8]. He also compared ASPEN HYSYS and ASPEN PLUS simulation of CO_2 Absorption into MEA from atmospheric gas in the same year [9].

Since 2013, a new option (ACID GAS package) is added to ASPEN HYSYS software that its producer claims this package uses rigorous rate-based calculations and a new property package to deliver unprecedented accuracy and predictive results to amine-based absorption processes [10]. This paper investigates mentioned claim and provides a comparison between the thermodynamic packages of ASPEN PLUS (V8.2) and ASPEN HYSYS (V8.3) in predicting the solubility of acid gases in amine solutions.

2. THEORETICAL FOUNDATIONS

Using thermodynamic relations based on classical concepts of phase equilibriums is an approach resulting in the prediction of acid gases solubility in aqueous alkanolamine solutions. However, the use of parameters such as fugacity and activity is more close to the physical senses than theoretical concept of chemical potential.

For each component in the mixture, the fugacity equality of liquid and vapor phases resulted from thermodynamic equilibrium, provides the possibility of using distinct thermodynamic models for the phases. Therefore, an equation of state will be used for predicting the vapor phase fugacity coefficients, while an activity model is used for the liquid phase. In the following, the calculation methods of vapor-liquid equilibrium condition by equations of state and activity model in thermodynamic packages of ELECNRTL and ACID GAS are discussed.

A. ELECNRTL Thermodynamic Package

One of the methods to predict the equilibrium behavior of electrolyte solutions is the activity coefficient model-based approach, which is established based on calculating the activity coefficients of the components in the

liquid phase. As mentioned, the ELECNRTL thermodynamic package that is an example of this approach, embedded in ASPEN PLUS software, was studied according to the purposes of this investigation. In this thermodynamic package, the Redlich-Kwong equation of state (RK) was selected to calculate the fugacity coefficient of components in the vapor phase.

But what has distinguished this thermodynamic package compared to other similar types, is the use of modified Electrolyte NRTL model to calculate the activity coefficients of the components in the liquid phase. The model proposed by Chen et al. [11], introduces the amount of excess Gibbs energy of the components in non-ideal electrolyte solutions, including two main parts that one is related to the local molecules and ions interactions (LI), and the other is related to Long-Range Ion-Ion Interaction (LR). It should be noted that in predicting the equilibrium behavior of electrolyte solutions, determining the ionic components amounts is of great importance, which is usually done by defining ionization reactions with inclusion of synthetic data or equilibrium constants. Kinetic and equilibrium data of these reactions are presented in [12].

In ASPEN PLUS software, several databases are available for thermodynamic calculations, which provide the possibility of using a different set of interaction parameters of ELECNRTL model and Henry constants. Among them, three special packages, namely as KEMDEA (Kinetic Equilibrium MDEA), KMDEA (Kinetic MDEA) and PMDEA (Posey MDEA) were imbedded that each would be used tailored to a specific usage and given the limits of experimental conditions for MDEA solutions. The calculation basis of components activity coefficients in the liquid phase is the Electrolyte NRTL model for all the packages which their interaction parameters have been recalled from different databases. The main difference between the KMDEA and KEMDEA packages is in the equation of state used for gas phase, so that the RK equation of state was used in the KEMDEA model, while the SYSOP15M equation of state was used in the KMDEA model. The PMDEA model developed based on the results of Posey et al. (1997) studies has considered two parameters of PH and electrical conductivity coefficient of the solution in estimating Henry constant parameters in order to eliminate measurement error of acid gases solubility, especially at low solubility rates [13]. Since the poor solubility changes can cause significant changes in PH and the value of solution electrical conductivity, thus, less error would occur in the measurement values. Finally, by including the PH and electrical conductivity, Posey and Rochelle provided new parameters for the calculation of Henry constants. In this study, three ELECNRTL thermodynamic packages of ASPEN PLUS software, name as KEMDEA, GLOBAL and PMDEA are selected for comparison. It should be noted that the GLOBAL database includes default values of the software.

The accuracy of estimation of mole fraction of molecular and ionic components considered in the equations in activity models are based on the accuracy of kinetic data and equilibrium constants of the existing chemical reactions. The ASPEN PLUS software package uses several reactions for ionization of acidic components and amine solutions that is presented in [12].

B. ACID GAS Thermodynamic Package

This package imbedded in ASPEN HYSYS for prediction of electrolyte solutions equilibrium behavior. This package has used the Electrolyte NRTL model to calculate the activity coefficients of the components in the liquid phase and the Peng-Robinson equation of state to calculate the vapor phase fugacity coefficient. The mentioned thermodynamic package have been developed merely for simulating the natural gas sweetening processes. In this thermodynamic package, according to recent studies, the possibility of using and examining the mixed amines has been also provided, and the relevant parameters have been calculated for each compound separately (Such as MDEA- PZ, Sulfolane-DIPA and MDEA-Sulfolane). The most important difference between ACID GAS thermodynamic package and the ELECNRTL package of ASPEN PLUS is in the set of interaction parameters used for each pair of molecules and ions.

3. RESULT AND DISCUSSION

A wide range of experimental data is needed to support validation of thermodynamic packages (ACID GAS, ELECNRTL). Since 1930 a large number of experimental solubility data for H_2S and CO_2 in aqueous amine has been published and presented by several investigators. Table 1 gives and overview on the previous results for these gases solubility in MDEA solution which are used for validating the selected thermodynamic packages. Where PH_2S and PCO_2 are the partial pressures of H_2S and CO_2, respectively.

A. Acid gas Solubility in MDEA Solutions

In this section, the simulation results of an acid gas-MDEA equilibrium stage (flash drum) by mentioned packages included in the ASPEN PLUS (KEMDEA, PMDEA, and GLOBAL MDEA) and ASPEN HYSYS (ACID GAS) which compared with experimental data are shown in Figures 1 to 10. The Average Absolute Deviation (AAD) for each thermodynamic package is also shown in Table 2.

A.1. Individual Acid Gas Solubility in Aqueous MDEA

Evaluation the solubility of CO_2 in the MDEA solution in absence of H_2S shows that the special data package of PMDEA compared to other ASPEN PLUS packages has a better estimation capability. However, the ACID GAS package predicts the CO_2 solubility as well as PMDEA (Figure 1).

The results of H_2S solubility in MDEA solution in absence of CO_2 indicate the lower accuracy of ACID GAS package compared to other packages. Assessment of results in Figure 2 shows that the error has occurred in high acid gas solubility. But in the low range of solubility, the results obtained from the thermodynamic ACID GAS package have enough accuracy.

A.2. Solubility of CO_2 and H_2S Simultaneously in Aqueous MDEA Solutions

Since in sweetening processes, both H_2S and CO_2 are usually present in the sour gas stream, thus, investigating the estimating ability of their interaction effect on solubility by thermodynamic packages is of utmost importance.

The results presented in Figures 3 to 10 demonstrate the ability to predict the H_2S and CO_2 solubility by ACID GAS package in low acid gases loading values. However, increasing this parameter (loading) will reduce the accuracy of solubility predicting by ACID GAS package compared to others. Also, this investigation shows that with increasing the mole fraction of CO_2 in sour gas (0.02-0.98), the results of PMDEA, KEMDEA and GLOBAL-MDEA packages will be partially better than ACID GAS package.

Table1. Literature data of acid gases solubility in aqueous MDEA solutions which are used in this paper for validating thermodynamic packages

Ref	Amine Concentration (wt. %)	Total Pressure (kPa)	Temp. (K)	P_{CO2} (kPa)	P_{H2S} (kPa)	Data NO.
[14]	MDEA (25.73%)	546.08-4386.8	313.17	533.9-4369.7	-	7
[15]	MDEA (46.78%)	6.21-1040.0	313.16	-	0-1000	13
[16]	MDEA (50%)	518-1999	323.15	10-1153	6-680	18
[17]	MDEA (50%)	200-8800	313.15	0.08-8120	0.295-2390	11
[18]	MDEA (35%) MDEA (50%)	690-7010 690-6990	298.15 298.15	0.3-10.12 0.62-14.9	0.19-15.2 0.19-11.3	18 18
[19]	MDEA+PZ (24, 0.08%) MDEA+PZ (24, 0.08%)	- -	313.15 333.15	0.10-95.3 0.08-83.1	- -	4 5
[20]	MDEA+PZ (47, 5 %) MDEA+PZ (47, 5 %)	- -	313.15 343.15	0.03-7.48 0.03-3.60	- -	4 3

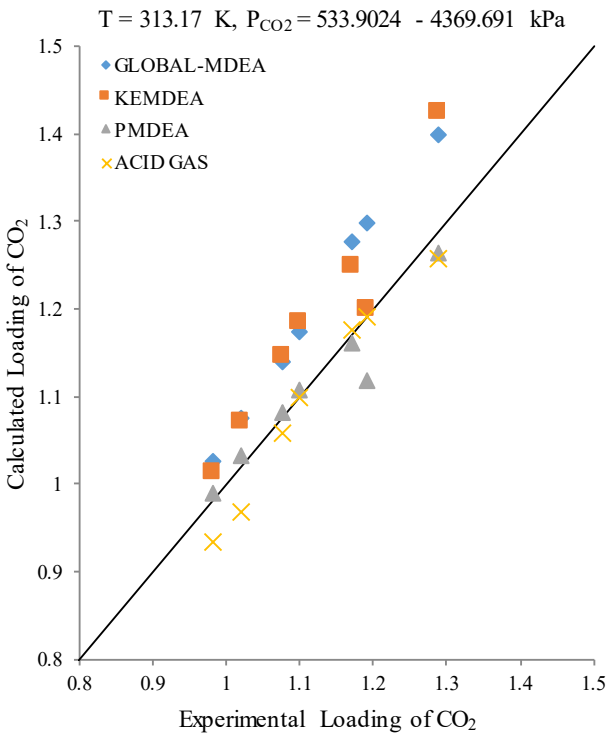

Figure 1. CO_2 solubility in MDEA (25.73wt.%)/CO_2 mixture at 313.17K [14]

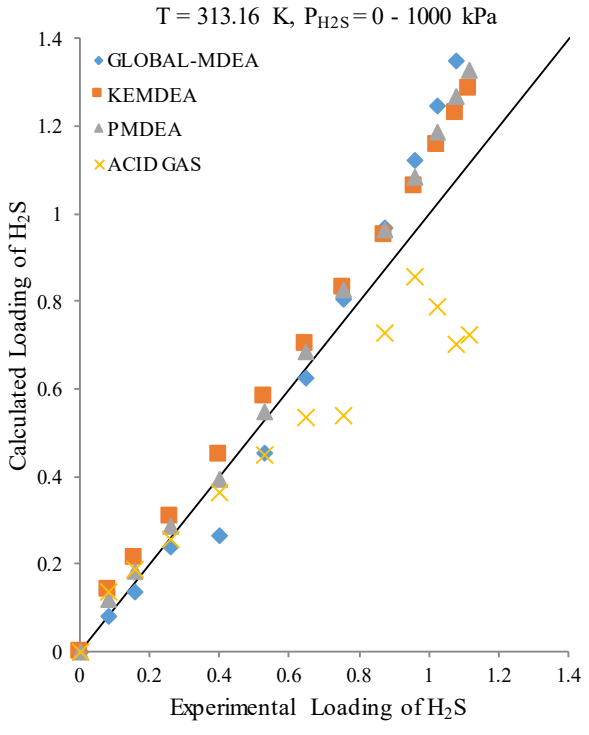

Figure 2. H_2S solubility in MDEA (46.78wt.%)/CO_2 mixture at 313.16K [15]

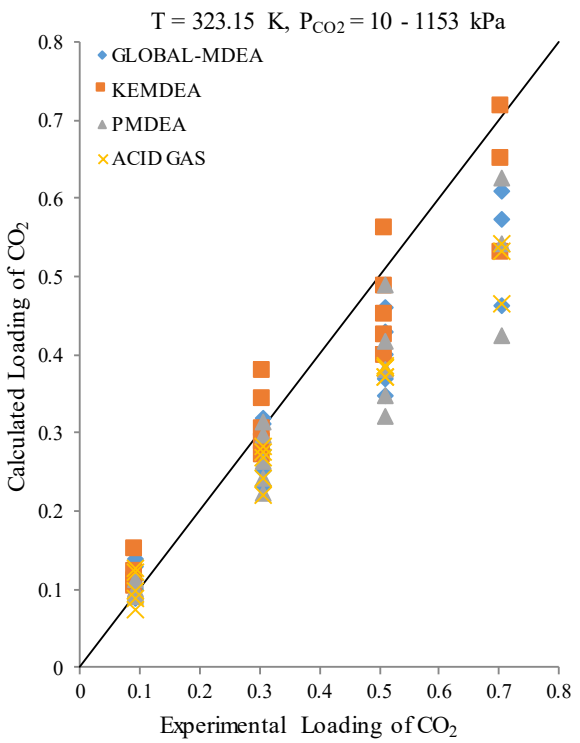

Figure 3. CO_2 solubility in MDEA (50 wt. %)/H_2S/CO_2 mixture at 323.15K [16]

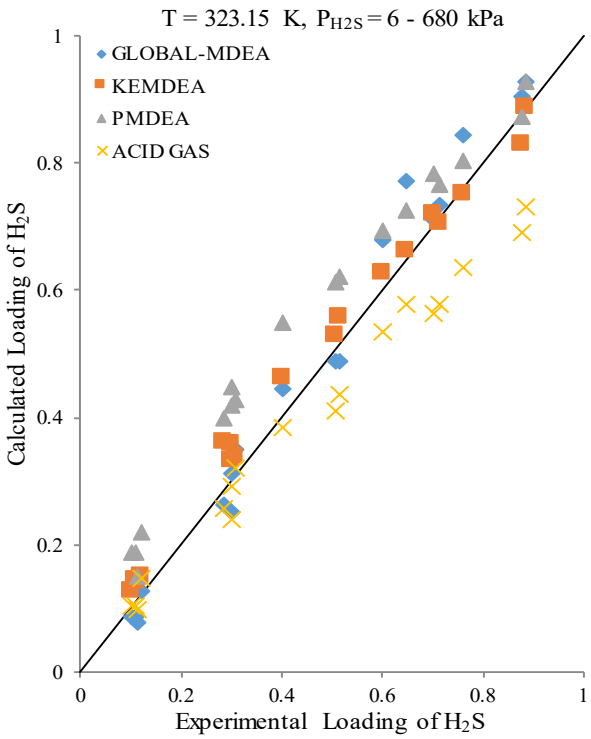

Figure 4. H_2S solubility in of MDEA (50 wt. %)/H_2S/CO_2 mixture at 323.15K [16]

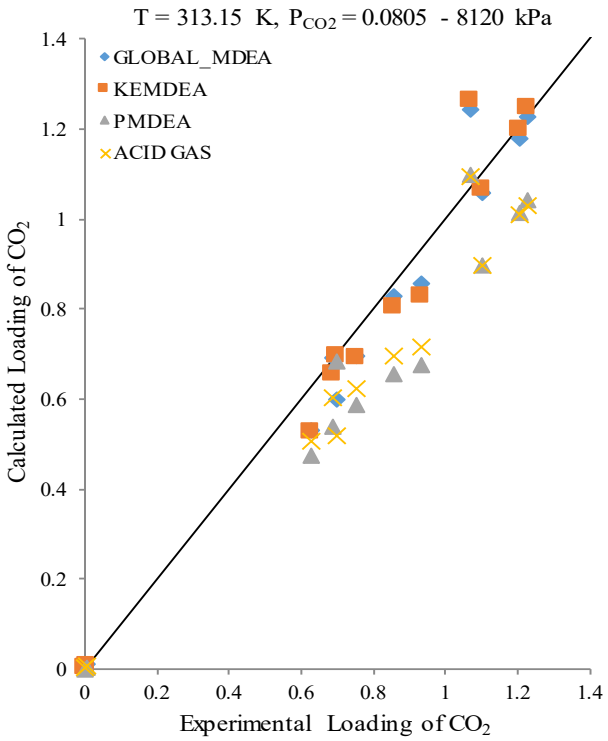

Figure 5. CO_2 solubility in MDEA (50 wt. %)/H_2S/CO_2 mixture at 313.15K [17]

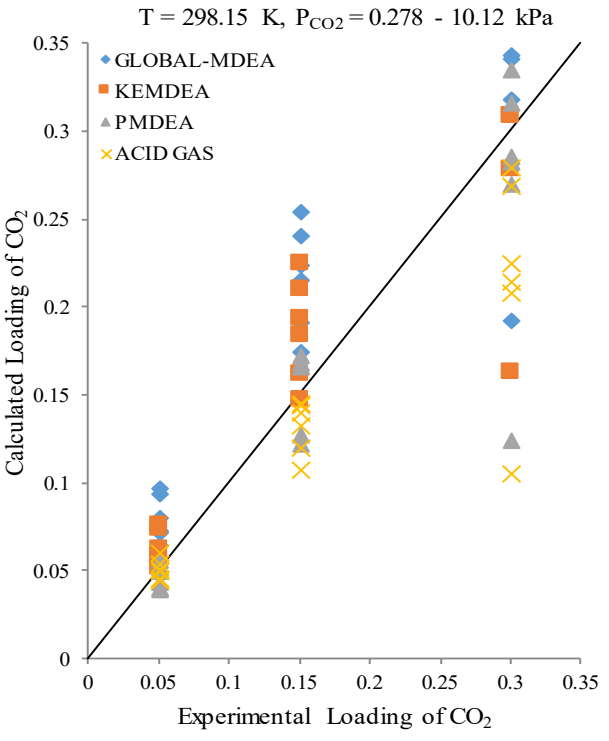

Figure 7. CO_2 solubility in MDEA (35wt.%)/H_2S/CO_2 mixture at 298.15K [18]

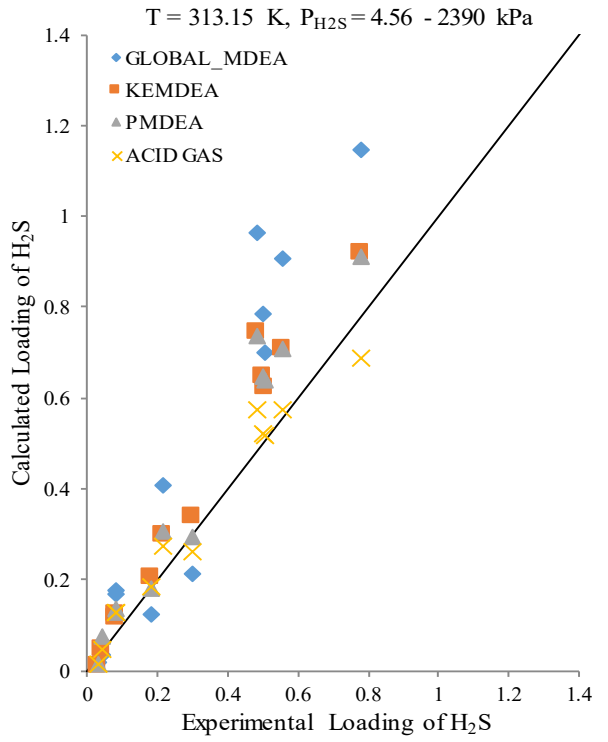

Figure 6. H_2S solubility in of MDEA (50 wt. %)/H_2S/CO_2 mixture at 313.15K [17]

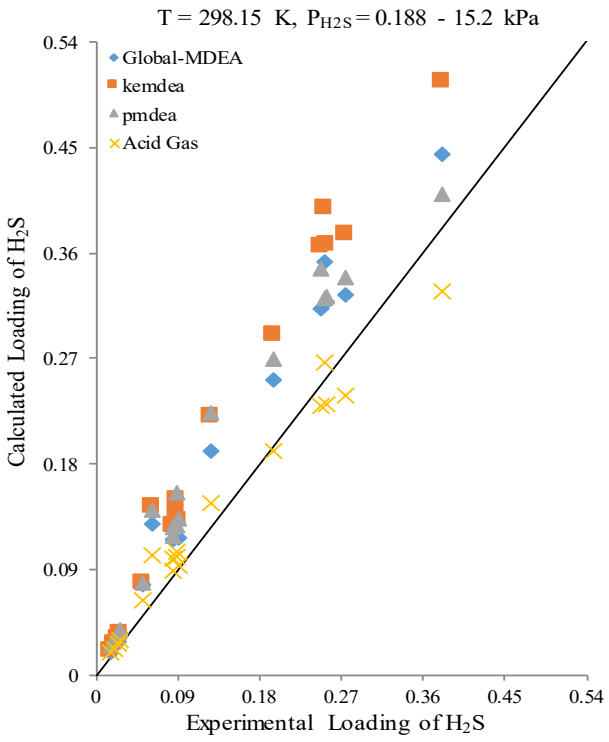

Figure 8. H_2S solubility in of MDEA (35wt.%)/H_2S/CO_2 mixture at 298.15K [18]

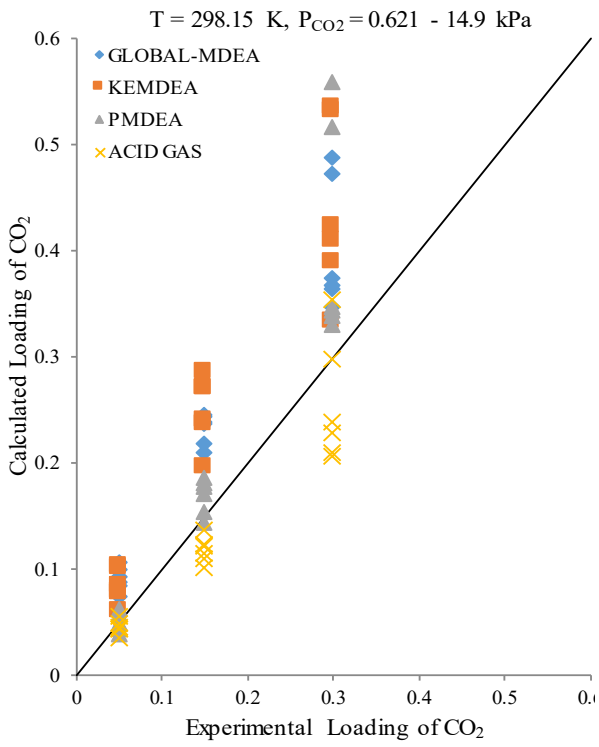

Figure 9. CO_2 solubility in MDEA (50wt.%) / H_2S/CO_2 mixture at 298.15K [18]

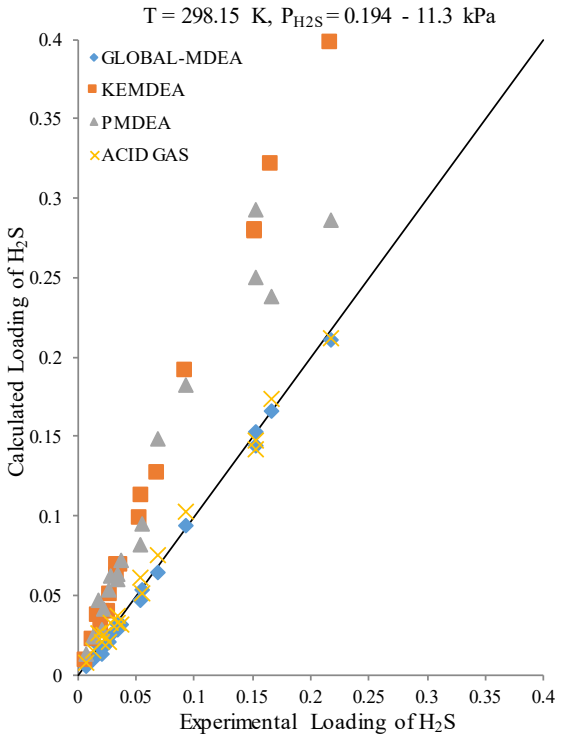

Figure 10. H_2S solubility in of MDEA (50wt.%)/H_2S/CO_2 mixture at 298.15K [18]

B. CO_2 Solubility in MDEA/PZ Solutions

In this section, the simulation results of an acid gas-MDEA/PZ equilibrium stage (flash drum) by GLOBAL MDEA/PZ (ASPEN PLUS) and ACID GAS (ASPEN HYSYS) which compared with experimental data are shown in Figures 11 to 14. The Average Absolute Deviation (AAD) for each thermodynamic package is also shown in Table 2.

The results shown in Figures 11 and 12, suggests the weakness of ACID GAS package in predicting of CO_2 solubility in activated amine solution. It is important to notice that, in Figures 11 and 12, the mass fraction of Piperazine in the solution is less than 1%, while industrial reports indicate that the mass fraction of Piperazine in gas sweetening processes is between 3% and 7%. According to the ASPEN TECH Company's claim regarding the enhancement of the ACID GAS thermodynamic package, a collection of experimental points based on gas processing operational data were used to tuning the ACID GAS package [10].

The results shown in Figures 13 and 14 indicate that by increasing the Piperazine concentration to 5 weight percent (gas processing operational range) the accuracy of CO_2 solubility prediction by ACID GAS package is also increased. However, the estimation capability of CO_2 solubility by ASPEN PLUS thermodynamic packages greatly reduced with increasing concentration of Piperazine more than 1 percent.

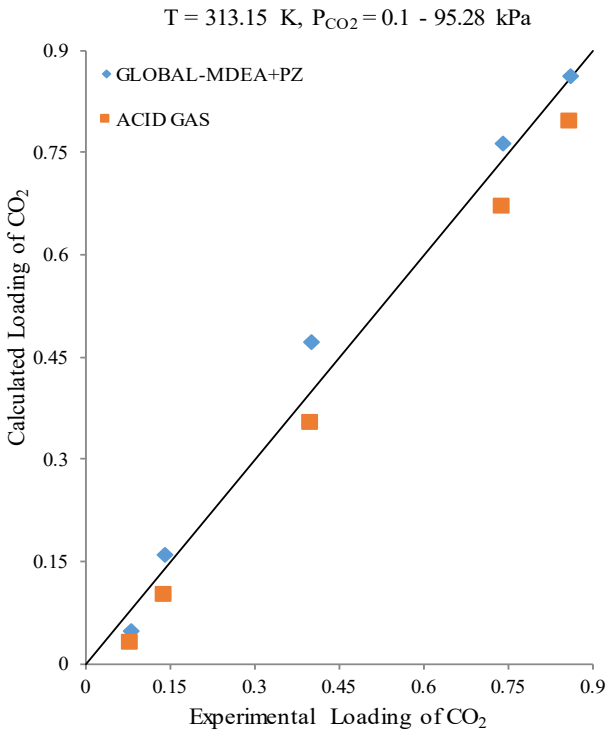

Figure 11. CO_2 solubility in of MDEA (24wt.%)/PZ (0.08wt.%)/CO_2 mixture at 313.15K [19]

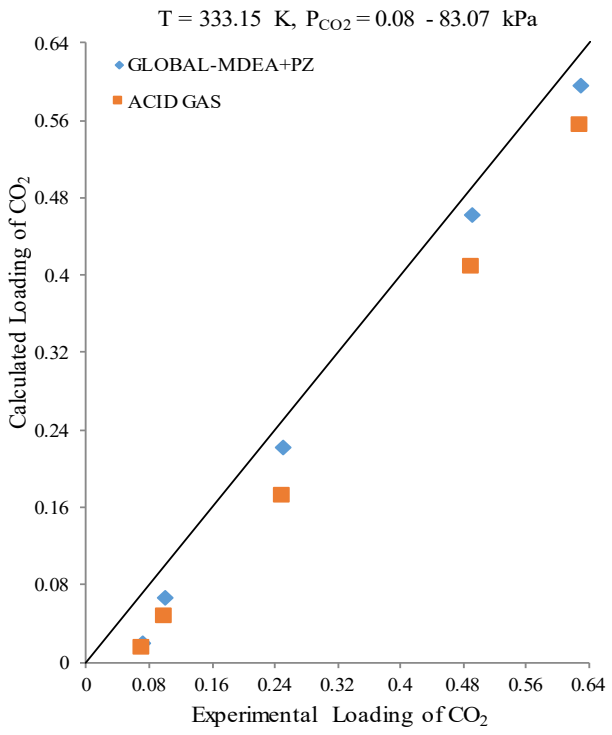

Figure 12. CO_2 solubility in of MDEA (24wt.%)/PZ (0.08wt.%)/CO_2 mixture at 333.15K [19]

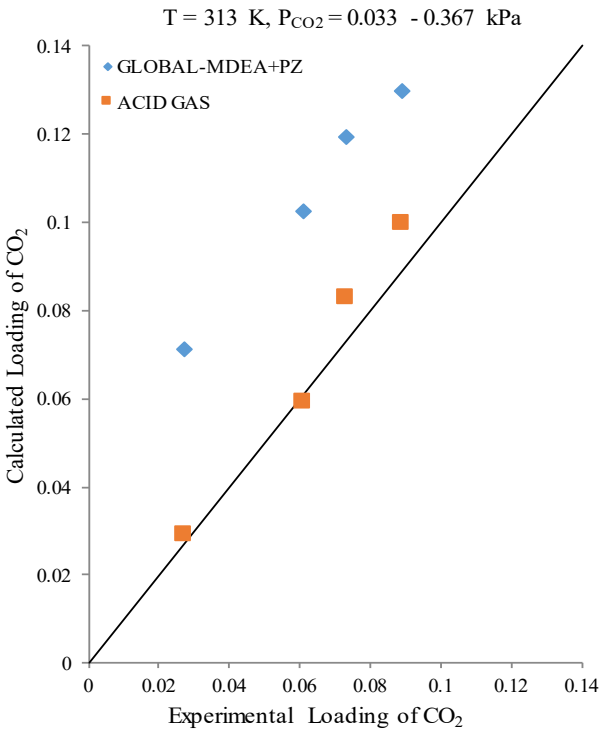

Figure 13. CO_2 solubility in of MDEA (47wt.%)/PZ (5wt.%)/CO_2 mixture at 313.15K [20]

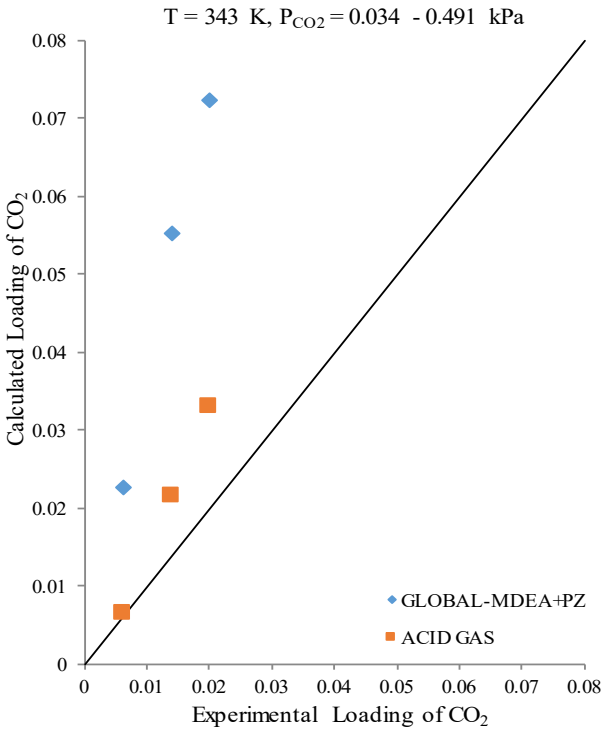

Figure 14. CO_2 solubility in of MDEA (47wt.%)/PZ (5wt.%)/CO_2 mixture at 343.15K [20]

Table 2. The Average Absolute Deviation of ELECNRTL and ACID GAS models in comparison with experimental data

Reference of experimental data	Figure	Model	(AAD) H_2S loading	(AAD) CO_2 loading
[14]	1	GLOBAL MDEA KEMDEA PMDEA ACID GAS	---- ---- ---- ----	7.1 5.8 1.8 2.4
[15]	2	GLOBAL MDEA KEMDEA PMDEA ACID GAS	15.5 18.9 13.9 22.2	---- ---- ---- ----
[16]	3	GLOBAL MDEA KEMDEA PMDEA ACID GAS	10.5 12.7 32.7 12.8	---- ---- ---- ----
[16]	4	GLOBAL MDEA KEMDEA PMDEA ACID GAS	---- ---- ---- ----	19.3 15.9 16.4 21.6
[17]	5	GLOBAL MDEA KEMDEA PMDEA ACID GAS	61.0 32.9 38.8 23.0	---- ---- ---- ----
[17]	6	GLOBAL MDEA KEMDEA PMDEA ACID GAS	---- ---- ---- ----	16.5 9.2 15.6 22.7
[18]	7	GLOBAL MDEA KEMDEA PMDEA ACID GAS	37.1 52.8 49.5 15.3	---- ---- ---- ----
[18]	8	GLOBAL MDEA KEMDEA PMDEA ACID GAS	---- ---- ---- ----	42.6 23.1 13.8 16.2
[18]	9	GLOBAL MDEA KEMDEA PMDEA ACID GAS	14.2 75.6 78.9 10.3	---- ---- ---- ----
[18]	10	GLOBAL MDEA KEMDEA PMDEA ACID GAS	---- ---- ---- ----	56.9 60.1 20.9 18.3
[19]	11	GLOBAL MDEA+PZ ACID GAS	---- ---- ---- ----	24.0 34.1
[19]	12	GLOBAL MDEA+PZ ACID GAS	---- ----	22.5 34.5
[20]	13	GLOBAL MDEA+PZ ACID GAS	---- ----	84.9 8.9
[20]	14	GLOBAL MDEA+PZ ACID GAS	---- ----	277.3 41.9

4. CONCLUSION

In this study, the prediction accuracy of H_2S and CO_2 solubility in aqueous MDEA and MDEA/PZ solutions has been investigated by using of two different packages of ASPEN PLUS and ASPEN HYSYS softwares (ELECNRTL and ACID GAS). The results showed that using of ACID GAS thermodynamic package has more accuracy specially for predicting the solubility of acid gases (at low concentration range) in MDEA solution, while, increasing the acid gas loading (specially CO_2 loading) will reduce the accuracy of solubility modeling by ACID GAS package compared to PMDEA, KEMDEA and GLOBAL-MDEA packages. The results also show that CO_2 solubility prediction by ACID GAS package is more accurate compared to GLOBAL-MDEA/PZ package when the Piperazine concentration is in the operational range of gas sweetening processes (3 to 7 wt. %).

ACKNOWLEDGMENT

This project was carried out within the research stream on optimization studies of BIDBOLAND gas refinery. The authors wish to thanks the refinery research unit officials for their valuable contributions, financial support of this research project and providing all necessary operating information.

REFERENCES

1. R. Deshmukh, A. E. Mather, "A mathematical model for equilibrium solubility of hydrogen sulfide and carbon dioxide in aqueous alkanolamine solutions," Journal of Chemical Engineering Science, Vol. 36, pp. 355-362, 1981.

2. M. Posey, K. G. Tapperson, G. T. Rochelle, "A simple model for prediction of acid gas solubilities in alkanolamines," Journal of Gas Separation and Purification, Vol. 1, pp. 181-186, 1996.

3. P. Patil, Z. Malik, M. Jobson, "Prediction of CO_2 and H_2S Solubility in aqueous MDEA solutions using an extended Kent and Eisenberg model," Institution of Chemical Engineers Symposium Series, Vol. 152, pp. 498-510, 2006.

4. P. Huttenhuis, N. J. Agrawal, G. F. Versteeg, "Solubility of Carbon Dioxide and Hydrogen Sulfide in Aqueous N-Methyldiethanolamine Solutions," Journal of Industrial and Engineering Chemistry, Vol. 48, pp. 4051-4059, 2009.

5. Y. Zhang, H. Que, C. C. Chen, "Thermodynamic modelling for CO_2 absorption in Aqueous MEA Solution with electrolyte NRTL model," Journal of Fuel and Energy Abstracts, Vol. 311, pp. 67-75, 2011.

6. Y. Zhang, C .C. Chen, "Thermodynamic modelling for CO_2 absorption in Aqueous MDEA Solution with electrolyte NRTL model," Journal of Industrial and Engineering Chemistry, Vol. 50, pp. 163-175, 2011.

7. E. Hansen, "Aspen HYSYS and Aspen Plus simulation programs for CO_2 absorption," Master's thesis, Telemark University College, Faculty of Technology, 2011.

8. L. E. Øi, "Removal of CO_2 from exhaust gas," M. C. Melaaen, revision of Ph.D. Dissertation Telemark University College Faculty of Technolo at porsgrumm, Norway, 2012.

9. L. E. Øi, "Comparison of Aspen HYSYS and Aspen Plus simulation of CO_2 absorption into MEA from atmospheric gas," Journal of Energy procedia, Vol. 23, pp. 360-369, 2012.

10. Optimize the entire gas process with acid gas cleaning. Available at: http://www. Aspentech .com/ products/V8-releash-prior, August 2013.

11. C .C. Chen, H. I. Britt, J. F. Boston, L. B. Evans, "Local composition model for excess Gibbs energy of electrolyte systems," AIChE Journal, Vol. 28, pp. 588, 1982.

12. ASPEN Physical Property system, Physical Property Methods and Models, chap.11.1.

13. M. L. Posey, G. T. Rochelle, "A Thermodynamic Model of Methyldiethanolamine-CO_2-H_2S-Water," Industrial & Engineering Chemistry Research, Vol. 36, pp. 3944-3953, 1997.

14. R. S. Boumedine, S. Horstmann, K. Fischer, E. Provost, W. Furst, J. Gmehling, "Experimental determination of carbon dioxide solubility data in aqueous alkanolamine solutions," Fluid Phase Equilibria, Vol. 218, pp. 85-94, 2004.

15. R. S. Boumedine, S. Horstmann, K. Fischer, E. Provost, W. Furst, J. Gmehling, "Experimental determination of hydrogen sulfide solubility data in aqueous alkanolamine solutions," Fluid Phase Equilibria, Vol. 218, pp. 149-155, 2004.

16. M. Dicko, C. Coquelet, C. Jarne, S. Northrop, D. Richon, "Acid gases partial pressures above a 50 wt% aqueous methyldiethanolamine solution: Experimental work and modelling," Fluid Phase Equilibria, Vol. 289, pp. 99-109, 2010.

17. F. Y. Jou, F. Otto, A. Mather, "The solubility of mixtures of H_2S and CO_2 in an MDEA solution," The Canadian Journal of Chemical Engineering, Vol. 75, pp. 1138-1141, 1997.

18. P. Huttenhuis, N. J. Agrawal, G. F. Versteeg, "Solubility of carbon dioxide and hydrogen sulfide in aqueous N-methyldiethanolamine solutions," Industrial & Engineering Chemistry Research, Vol. 48, pp. 4051-4059, 2009.

19. B. S. Ali, M. K. Aroua, "Effect of piperazine on CO_2 loading in aqueous solutions of MDEA at low pressure," International Journal of Thermophysics, Vol. 25, pp. 1863-1870, 2004.

20. S. Bishnoi, G. T. Rochelle, "Thermodynamics of piperazine/methyldiethanolamine/water/carbon dioxide," Industrial & Engineering Chemistry Research, Vol. 41, pp. 604-612, 2002.

Investigation on Solubility of Hydrogen Sulfide in Molten Sulfur Using Iodometric Back Titration Method

• **Faezeh Tari[1], Marzieh Shekarriz [1*], Saeed Zarrinpashne[2], Ahmad Ruzbehani[1]**

1. Chemical, Polymeric and Petrochemical Technology Research Division, Faculty of Research and Development in Downstream Petroleum Industry, Research Institute of Petroleum Industry (RIPI), P.O. Box 1485733111, Tehran, Iran
2. Gas Technology Research Division, Faculty of Research and Development in Downstream Petroleum Industry, Research Institute of Petroleum Industry (RIPI), Tehran, Iran

Corresponding author Email address: Shekarriz@ripi.ir

Received: Feb. 27, 2017 / Accepted: Apr. 29, 2017

Abstract

In order to conduct laboratory studies on composition and behavior of Claus-derived molten sulfur, the examined sulfur should contain dissolved H_2S and H_2Sx with a concentration of about 230-250ppmw. Here, by injecting hydrogen sulfide to sulfur, a method for synthesis of molten sulfur containing hydrogen sulfide and polysulfide as a proper sample for laboratory studies is developed. The molten sulfur as product was prepared by injecting the pressurized hydrogen sulfide on the surface of solid sulfur followed by further heat treatments during the time. According to the Iodometric Back Titration (IBT) analysis, final molten sulfur contained 500-1100ppmw of soluble hydrogen sulfide and polysulfide components based on the initial gas pressure.

Keywords: Molten sulfur, Gassing, Degassing, Iodometric Back Titration

1. Introduction

Claus units in refineries are used for processing the sour gas as the byproduct of gas sweetening process [1]. Passing through the combustion chamber, the sour gas components are converted to sulfur vapors and non-reacted gases. Then, after separation and condensation of sulfur in special condensers, the remained gases are moved to Claus catalytic beds, where catalytic reactions took place and collection of condensate sulfur continues [2].

Usually, pure sulfur at atmospheric pressure and temperatures higher than its melting point (118°C) is available in the form of S_8 with ring structure. At temperatures higher than 148°C, sulfur structure is converted to straight chains. According to Eq. 1 this phenomenon leads to generation of polymeric chains with different length and sometimes of thousands of units [3].

$$S_8(ring) \rightarrow \left(\frac{x}{8}\right) S_8(straight\ chain) \rightarrow S_x\ (Polymeric) \quad (1)$$

Formation of such polymeric chains in the condensers of Claus unit causes a complex physicochemical interaction between the dissolved hydrogen sulfide and molten sulfur .In fact there is an equilibrium relation between the hydrogen sulfide in the gas phase and hydrogen sulfide dissolved in the liquid phase, which is a kind of equilibrium solubility of gases dominant in liquid-gas systems. This relationship is reversible depending on the partial pressure of hydrogen sulfide in the gas phase and temperature of liquid sulfur.

Equilibrium exchange of hydrogen sulfide between gas and liquid phases is fast, while the dissolved hydrogen sulfide can react with the polymeric chains in molten sulfur and form polysulfide components [4-6]:

$$H_2S\,(vap) \leftrightarrow H_2S\,(liq) \quad \text{(Fast)} \quad (2)$$

$$H_2S\,(liq) + S_{x-1} \leftrightarrow H_2S_x \quad \text{(Slow)} \quad (3)$$

As mentioned before formation of polysulfide species in the solution is relatively fast, while decomposition of them is usually very slow. Finally, a mass of molten sulfur is collected in storage tanks containing hydrogen sulfide and hydrogen polysulfide with a concentration of about 250-350 ppmw. Since it is necessary to pass the product sulfur via granulation unit before sending to the market, existence of sulfide and polysulfide cause problems and risks at this step. Because high temperature of the process prevents the transfer of hydrogen sulfide from liquid phase to gas phase, but at lower temperatures (in storage tanks), polysulfide components are decomposed and release hydrogen sulfide. In fact, the equilibrium reactions of (3) and (2) are moved to left side, respectively and hydrogen sulfide is immediately moved to gas phase. In this condition, gas accumulation in enclosed space causes problems like poisoning and explosion. Hence, some methods are presented by scholars for reduction of hydrogen sulfide concentration in molten sulfur before entering the grading units aiming to break the polysulfide chains and reduce the concentration of hydrogen sulfide until the concentration of about 10ppmw [5-7].

The main problem in investigation of degassing methods in laboratory scale is lack of access to molten sulfur of the Claus unit, because transportation of such material is very difficult and dangerous, due to release of hydrogen sulfide.

In this regard, some methods are reported by the researchers to study the interaction of hydrogen sulfide and molten sulfur. For example, Fanelli [8] studied the solubility of hydrogen sulfide in molten sulfur by measuring the weight difference and concluded that solubility of hydrogen sulfide in molten sulfur is increased by increase of temperature. He also showed that solubility of hydrogen sulfide in molten sulfur changes the viscosity of molten sulfur and attributed it to formation of polysulfide species.

Then, Wiewiorowski and Touro [9] confirmed Fanelli's observations using Furrier Transform Infrared spectroscopy (FTIR) and attributed the different generated peaks to hydrogen sulfide and polysulfide.

Marriott et al. [10] also studied the solubility of hydrogen sulfide in molten sulfur using hydrogen sulfide gas flow diluted by nitrogen gas at the pressures lower than 1 bar and finally derived a correlation representing the ratio of hydrogen polysulfide to hydrogen sulfide species in the solution.

Ji et al. [11] used a laboratory system to investigate the solubility of hydrogen sulfide in molten sulfur and derived the diffusion coefficients of hydrogen sulfide in molten sulfur and rate constants of Eq. 3 at 130°C and 150°C. But because it took a long time to reach the equilibrium state, they applied a regression equation to predict the equilibrium pressure.

Here, we apply a method to investigate the equilibrium condition at pressures higher than 1bar to produce molten sulfur containing specific concentration of hydrogen sulfide and polysulfide which was then detected by IBT method. The prepared sample can be used for degassing operations at laboratory scale.

2. Experimental

2.1. Materials and Equipment

Pure sulfur (99%, Tehran refinery), hydrogen sulfide cylinder (99%, Roham Gas), cadmium acetate dehydrate (Merck), 0.05M iodine standard solution (Sigma Aldrich), sodium thiosulfate (Sigma Aldrich), starch solution, hydrochloric acid (Merck) were used as reagents. A 250mL jacketed steel reactor equipped with hot oil circulator, magnetic stirrer, pressure gauge (-1:10bar, Wika), hydrogen sulfide analyzer (7H CiTiceL, UK) were also used to conduct the experiments.

2.2. Dissolution of H_2S in Molten Sulfur

200g of solid sulfur with density of 2g/cm^3 was put into the reactor (Figure 1) and then reactor was evacuated until -0.9barg to remove excess air in the vessel. Hydrogen sulfide was injected to the reactor from a top valve until the total pressure reached to about 3barg. Reactor temperature was raised and fixed at 150°C using the hot oil circulator system. Then it was allowed to reach equilibrium under 200 rpm stirring followed by stabilization of system pressure. After reaching the equilibrium state, system was left for 24 hours in order to form polysulfide. After desired time, system pressure was lowered to atmospheric pressure and released content of hydrogen sulfide was trapped in a solution of cadmium acetate (step 1). The hydrogen sulfide existed on the surface of molten sulfur also was stripped by nitrogen gas and trapped in the absorbent solution, until the concentration of detected hydrogen sulfide in H_2S analyzer became less than 1ppmw (step 2). Then, the absorbent solution was replaced by a fresh solution of cadmium acetate. Again, by sparging nitrogen gas into the molten sulfur, the color of trap solution was changed slowly to pale yellow and this process was continued for about 6-7 hours, as concentration of detected hydrogen sulfide in gas phase reached lower than 1ppmw (step 3). Trap solutions were analyzed by Iodometric Back Titration (IBT) for quantitative studies.

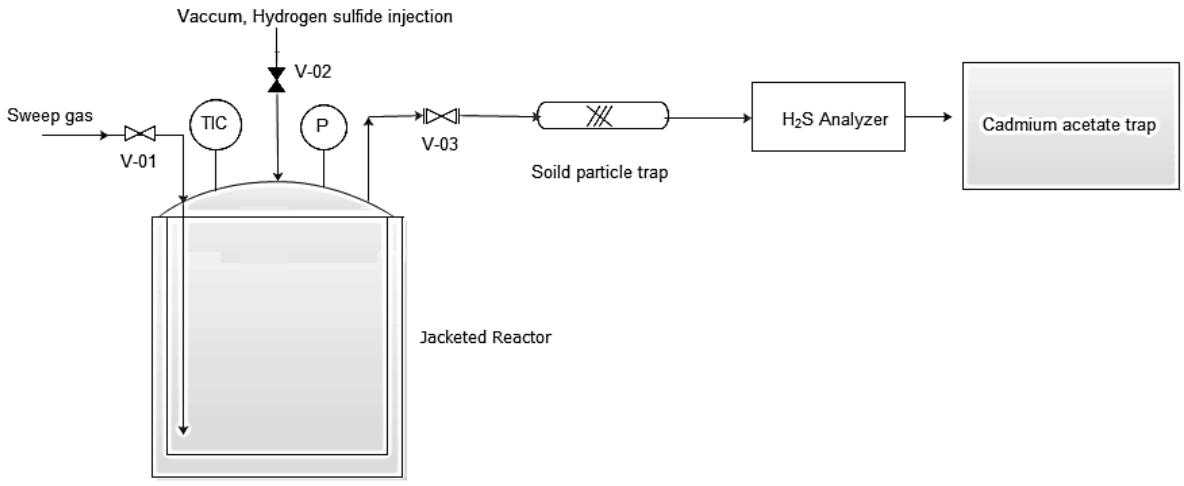

Figure.1. Molten sulfur gassing system

2.3.Iodometric Back Titration

For standardization, 25 ml of the 0.1N iodine solution was pipette to the flask. The solution was then titrated with 0.1N solution of sodium thiosulfate until a clear endpoint. Then, excess amounts of a mixture of 37% hydrochloric acid and 0.1N standard iodine solution were added to the trap. After adding a drop of starch solution to the mixture as indicator, resulting solution was titrated by 0.1N sodium thiosulfate solution until the colorless point. The used volume of sodium thiosulfate solution was read for further calculations.

3.Results and Discussions

3.1. IBT analysis

3.1.1. Standardization

As mentioned above, concentration of hydrogen sulfide in each step was detected by analysis of cadmium acetate solution via Iodometric Back Titration (IBT) method based on interaction of hydrogen sulfide with excess iodine solution and titration by sodium thiosulfate. Before conducting the analysis, it is important to standardize the iodine and sodium thiosulfate solutions for accurate results. Accordingly:

A=normality of iodine solution × volume used (ml)
B=normality of sodium thiosulfate solution ×volume used (ml)
$F=B/A$

If the F factor was within the limits of 0.95-1.05, solutions were prepared accurately and can be used in IBT analysis. Else, solutions should be prepared again until the F factor lays within the desired range. In this work, standard solutions were obtained after two runs. Results are shown in Table 1.

Table 1. Results of Standardization

Run	Volume of iodine solution (ml)	Volume of sodium thiosulfate solution (ml)	A	B	F=B/A
1	25	23.5	2.5	2.35	0.94
2	25	24	2.5	2.40	0.96

3.2.2. IBT calculations

First, absorption of hydrogen sulfide in cadmium acetate solution led to formation of yellow precipitates of cadmium sulfide, as shown in Eq.6:

$$H_2S + Cd(CH_3CO_2)_2 \rightarrow CdS + 2(CH_3CO_2H) \quad (6)$$

Since stochiometric coefficients of hydrogen sulfide and cadmium sulfide are the same, the equal moles of cadmium sulfide would be generated.

Then, according to Eq. 7 and Eq. 8 addition of hydrochloric acid and excess iodine solution, led to liberation of hydrogen sulfide and generation of HI, respectively.

$$CdS + 2HCl \rightarrow H_2S + CdCl_2 \quad (7)$$

$$H_2S + I_2 \rightarrow 2HI + S \quad (8)$$

As shown above, addition of concentrated hydrochloric acid leads to liberation of hydrogen sulfide, which is immediately absorbed by iodine contents in the solution. Since iodine solution was used in excess values, some parts of non-reacted iodine ions remains in the environment. According to the literature [12], such excess values can be determined by titration of solution with sodium thiosulfate solution, which is standardized by iodine solution.

In continue, number of the excess iodine moles reacted with sodium thiosulfate solution (Eq. 9) was obtained by titration of solution in presence of starch solution [13].

$$2S_2O_3^{2-} + I_2 \rightarrow S_4O_6^{2-} + 2I^- \quad (9)$$

The number of iodine moles reacted with hydrogen sulfide are calculated as the difference of initial iodine moles and remained moles which reacted with sodium thiosulfate. Hence, the content of hydrogen sulfide moles in each step can be determined.

3.1 Gassing

First, by putting solid sulfur in the reactor with the density of 2 g/cm^3, 150 cm^3 of reactor space was remained for injection of hydrogen

sulfide. The initial number of hydrogen sulfide moles injected to the vessel was calculated according to Ideal gas law at 25°C and vessel pressure. So, this initial value should be equal to the sum of hydrogen sulfide moles in trap solutions of three steps, detected by Iodometric Back Titration (IBT).

As reported in literature [6-8], despite most of gas-liquid systems, solubility of hydrogen sulfide in molten sulfur increases with temperature. Such behavior may be attributed to formation of polysulfide species in liquid sulfur. In fact, since generation of polysulfide bonds is facilitated at higher temperatures, more hydrogen sulfide is dissolved in liquid sulfur. For further investigations, experiments were repeated at 2.5 bar and results are presented in Figure 2.

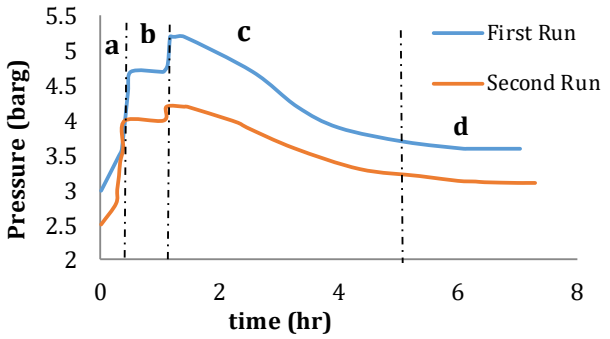

Figure 2. Pressure change rate of hydrogen sulfide in molten sulfur

According to Figure 2, in zone (a) gas pressure is increased due to of increase of system temperature. In zone (b), system pressure (and temperature) is fixed for a specific time, which indicates the phase change of solid sulfur to molten state. After complete melting of sulfur at about 120°C, system pressure was increased further until the temperature of whole system was fixed at 150°C (at the end of zone b). After reaching the maximum pressure and temperature, pressure decay process was initiated in zone (c), referring to dissolution of hydrogen sulfide in molten sulfur. Such trend was continued for a specific time and after reaching the equilibrium state (P_{eq}), system pressure was stabilized in zone (d). In fact, when reactor temperature was fixed at the equilibrium condition, it was allowed to form hydrogen polysulfide by interaction of sulfur free radicals with hydrogen sulfide dissolved in molten sulfur during 24 hours. According to Ji et al. [11] initial concentration of hydrogen sulfide in liquid sulfur can be derived by Eq. 5.

$$C = \frac{M(P_i - P_{eq})V_g}{RT m_s} \quad (5)$$

Where C is the concentration of hydrogen sulfide in molten sulfur, M is the molecular weight of hydrogen sulfide, P_i is the initial pressure of the vessel, P_{eq} is the vessel pressure at equilibrium condition, V_g is the gas injection volume, R is the gas constant, T is the vessel temperature and m_s is the weight of solid sulfur.

After reaching the equilibrium state, as mentioned above, un-reacted and excess hydrogen sulfide remained on the headspace of molten sulfur was discharged during steps 1&2. Such release was so fast and after some minutes, concentration of hydrogen sulfide in the stripper gas reached lower than 1ppmw, using H_2S analyzer. Regarding the fast release of gas from molten sulfur, it could be said that it was unbounded hydrogen sulfide. Hydrogen sulfide content released in these steps was trapped in cadmium acetate solution. Then, the orange trap solution containing cadmium sulfide was replaced by a fresh colorless solution of cadmium acetate. In continue, by sparge of nitrogen gas into the molten sulfur, gradual color change of trap solution was happened and continued for about 6-7 hours, where concentration of hydrogen sulfide detected by H_2S analyzer reached lower than 1ppmw (step 3). In this regard, despite steps 1&2, very slow rate of hydrogen sulfide release from solution can be attributed to decomposition of polysulfide species in the sample. The trap solutions of steps 1&2 and step 3 were analyzed by Iodometric Back Titration (IBT) method for determining the hydrogen sulfide content released in each step.

For more investigations, results obtained by Eq. 5 were compared to analytical results of Iodometric Back Titration (IBT) method, as shown in Table 2.

Table 2. Results of dissolution process

Run	Initial H_2S pressure (bar)	Initial H_2S (mol)	Maximum H_2S pressure (bar)	Equilibrium H_2S pressure (bar)	Un-bounded H_2S in steps 1&2 (mol)	H_2S in step 3	Calculated concentration of H_2S in molten sulfur according to IBT analysis (ppmw)	C(ppmw) according to eq.5
1	3	0.018	5.21	3.4	0.0118	0.0062	991	1100
2	2.5	0.015	4.2	3.2	0.0115	0.0035	560	624

As shown in Table 2, initial injection pressure of H_2S was used for estimation of initial (total) moles of hydrogen sulfide in the system. Maximum and equilibrium pressures of H2S were used for calculation of C (ppmw) according to eq. (5). H_2S content in step 3 was determined by Iodometric Back Titration (IBT) analysis of the second trap solution and then was applied for determination of dissolved hydrogen sulfide and polysulfide concentration in molten sulfur.

Clearly, the initial mole of injected hydrogen sulfide was equal to sum of moles of unbonded and bounded hydrogen sulfide in steps 1&2 and 3. In addition, the concentrations (ppmw) obtained by eq. (5) and dissolved hydrogen sulfide content at step 3 were in a good agreement, while the difference of about 50-100ppmw was also reported by other researchers [11].

4. Conclusions

Regarding the need to molten sulfur containing dissolved hydrogen sulfide and polysulfide in laboratories for studying different degassing methods, this article aims to investigate a gassing procedure at pressures higher than atmospheric. In this study, we applied pressures up to 3bars and allowed the system to reach equilibrium during the time. Outputs of system were analyzed by Iodometric Back Titration and compared with theoretical investigations. Results showed that there is a good agreement between results obtained via these two approaches. Therefore, we can conclude that molten sulfur containing dissolved hydrogen sulfide and hydrogen polysulfide components can be produced via this method and be used for further processing of degassing methods in the laboratory.

5. References

1. P.D. Clark. Fundamental and Practical Aspects of the Claus Sulfur Recovery Process, The Topsoe Catalysis Forum, 2007.
2. G. Mcintyre, L.Lyddon. Claus Sulphur Recovery Options, Petroleum Technology Quarterly Spring 1997: 57-61.
3. B. Meyer. Elemental Sulfur. Chemical Reviews, 1976, 76 (3) 367-388.
4. E. Nasato, T. Tex. Process for the high pressure degassing of hydrogen sulfide from liquid sulfur. Goar, Allison & Associates, Inc., US Patent 5632967, 1997.
5. J. G. Louie. Methods and apparatus for degassing liquid sulfur. Dynamax Engineering Ltd., Calgary (CA). US Patent 7081233B2, 2006.
6. P.T. Pendergraft, R.L. McGalliard. Process for removal of hydrogen sulfide and hydrogen polysulfide from liquid sulfur. Amoco Corporation. US Patent 4844720 1989.
7. P.T. Pendergraft. Process and apparatus for degassing sulfur. Amoco Corporation. US Patent 4729887, 1988.
8. R. Fanelli. Solubility of hydrogen sulfide

in sulfur. Ind. Eng. Chem., 1949 4 (9) 2031-2033.

9. T.K. Wiwiorowski and F.J. Touro. The sulfur-Hydrogen sulfide system. J. Phys. Chem. 1966 70 (1) 234-238.

10. R.A. Marriott, E.D. Fitzpatrick, K.L. Lesage. The solubility of H2S in liquid sulfur. Fluid Phase Equilib. 2008 269 69-72.

11. Y. Ji, H. Li, Z. Xu, Z. Tan. The diffusion coefficient of H_2S in liquid sulfur. Fluid Phase Equilib. 2011, 307, 135-141.

12. ANSI/NACE Standard TM0284-2003, Item No. 21215.

13. A. Roozbehani, F. Mohammadifard, F. Vakili, E. Alaie. Iodometric Back Titration method for hydrogen sulfide determination in Bitumen-Sulfur mixtures. 14th International Oil, Gas and Petrochemical Congress, 2010, 1-8.

Analysis of Counter-Current Imbibition Including Gravity Force through Finite Difference Scheme

· **Mojgan Ebrahiminejadhasanabadi[1], Mohammad Reza Ehsani[1*], Mahnaz Tayari[2], Mohammad Nikukar[3]**

1. Department of Chemical Engineering, Isfahan University of Technology, Isfahan, Iran
2. School of Chemical Engineering, University of Tehran, Tehran, Iran
3. Enhanced oil recovery Institute NIOC, Tehran, Iran

Corresponding author Email address: Ehsanimr@cc.iut.ac.ir

Received: Nov. 28, 2017 / Accepted: Jan. 22, 2018

Abstract

Spontaneous counter-current imbibition is one of the most important crude oil recovery processes in water-wet fractured reservoirs with low matrix permeability. This paper presents a numerical modeling of imbibition process when water is imbibed by capillarity and gravity forces in to an oil saturated vertical cube core to examine the effect of gravity force on spontaneous imbibition. In this modeling, it is assumed that imbibition is a diffusion process. Finite difference implicit method was used to solve the spontaneous imbibition equations. Accuracy of the modeling is investigated with comparison of the modeling results and the experimental data.

Keywords: Spontaneous imbibition, Counter-current imbibition, Oil recovery, Gravity force.

1. INTRODUCTION

Many attempts have been done to examine the imbibition's effective parameters. The fluids flow is complex in the fracture reservoirs, as the fluid can flow in the porous medium, that has low transmissibility and high capacity, and the narrow fracture, that has high transmissibility and low capacity. When the matrix is saturated with non-wetting phase and wetting-phase is in the fracture, the capillary and gravity forces cause displacement of wetting-phase into the porous medium, this process is called imbibition [1]. The imbibition process can be classified into two categories: co-current and counter-current flows. In the counter-current imbibition, oil and water flow in the opposite directions; in the co-current imbibition, water and oil flow in the same direction [2]. Blair (1964) modeled numerically the 1-dimentional counter-current imbibition process in a porous network and concluded that the rate of imbibition is sensitive to capillary pressure, relative permeability, oil viscosity and initial water saturation [3]. Beckner et al. (1987) modeled the imbibition process as a diffusion process. He assumed that diffusion coefficient is nonlinear and also gravity forces are ignored [4]. Behbahani et al. (2006) simulated spontaneous countercurrent imbibition in one and two-dimensional systems. The simulated results matched the experimental results reported by several authors, and they concluded that the conventional Darcy's law for multiphase flow was adequate to describe spontaneous countercurrent imbibition [2].

In this study, three-dimensional model is presented for study of spontaneous imbibition process. The two-phase mass balance equations for water and oil using Darcy's equation and other auxiliary equations are solved simultaneously by finite difference method. Then, this model is used to study the effect of gravity forces on imbibition performance.

2. MATHEMATICAL FORMULATION

A mathematical formulation of the spontaneously imbibition process is presented here. It is assumed that the fluids and core are incompressible. The model consists of two main equations containing of conservation mass equation for water and oil. Conservation mass equation for each phase (oil and water) in x, y and z directions in a cube core (Fig.1) is obtained as below:

$$\emptyset\frac{\partial(S_w)}{\partial t}+\frac{\partial(u_{wx})}{\partial x}+\frac{\partial(u_{wy})}{\partial y}+\frac{\partial(u_{wz})}{\partial z}=0 \quad (1)$$

$$\emptyset\frac{\partial(S_o)}{\partial t}+\frac{\partial(u_{ox})}{\partial x}+\frac{\partial(u_{oy})}{\partial y}+\frac{\partial(u_{oz})}{\partial z}=0 \quad (2)$$

Water and oil velocities can be obtained using Darcy's law as follow:

$$u_{hx}=\frac{-k_h}{\mu_h}\left(\frac{\partial P_h}{\partial x}-\rho g_x\right) \quad (3)$$

The total velocity for counter-current imbibition process is zero:

$$u_t=0 \quad (4)$$

$$u_{ox}+u_{wx}=0 \quad (5)$$

by inserting Darcy's equation in the Eq. (5):

$$\frac{-ko}{\mu o}\left(\frac{\partial P_o}{\partial x}-\rho g_x\right)+\frac{-kw}{\mu w}\left(\frac{\partial P_w}{\partial x}-\rho g_x\right)=0 \quad (6)$$

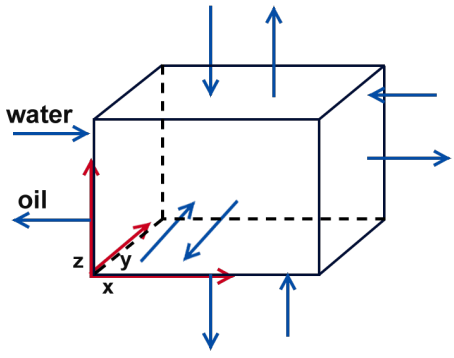

Figure. 1 Core geometry for the spontaneous imbibition when all faces are open

Auxiliary equations are the correlation between capillary pressure and water saturation that can be used to replace the capillary pressure

by saturation equations as follows:

$$P_{cw} = P_o - P_w = f(S_w) \tag{7}$$

Where,

$$\frac{\partial P_o}{\partial x} = \frac{\partial P_c}{\partial x} + \frac{\partial P_w}{\partial x} \tag{8}$$

By inserting Eq. (8) into Eq. (6):

$$\frac{\partial Pw}{\partial x} = -\frac{g_x\left(\frac{k_w}{\mu_w}\rho_w - \frac{k_o}{\mu_o}\rho_o\right) + \frac{k_o}{\mu_o}\frac{\partial Pc}{\partial x}}{\frac{k_o}{\mu_o} + \frac{k_w}{\mu_w}} \tag{9}$$

By substituting Eq. (9) into the Darcy's equation, the oil and water velocities are obtained as function of capillary pressure as follow:

$$u_{wx} = \frac{k_w k_o}{k_o\mu_w + k_w\mu_o}\left(g_x(\rho_w - \rho_o) + \frac{\partial Pc}{\partial x}\right) \tag{10}$$

$$u_{wy} = \frac{k_w k_o}{k_o\mu_w + k_w\mu_o}\left(g_y(\rho_w - \rho_o) + \frac{\partial Pc}{\partial y}\right) \tag{11}$$

$$u_{wx} = \frac{k_w k_o}{k_o\mu_w + k_w\mu_o}\left(g_z(\rho_w - \rho_o) + \frac{\partial Pc}{\partial z}\right) \tag{12}$$

Finally, by inserting above equations into Eq. (1), the governing equation for internal blocks will be obtained as follows:

$$\varphi\frac{\partial(sw)}{\partial t} + \frac{\partial\left(\frac{k_w k_o}{k_o\mu_w + k_w\mu_o}(g_x(\rho_w - \rho_o) + \frac{\partial Pc}{\partial x})\right)}{\partial x} + \frac{\partial\left(\frac{k_w k_o}{k_o\mu_w + k_w\mu_o}(g_y(\rho_w - \rho_o) + \frac{\partial Pc}{\partial y})\right)}{\partial y} + \frac{\partial\left(\frac{k_w k_o}{k_o\mu_w + k_w\mu_o}(g_z(\rho_w - \rho_o) + \frac{\partial Pc}{\partial z})\right)}{\partial z} = 0 \tag{13}$$

The capillary diffusivity coefficient (CDC) is defined as:

$$D(S_w) = -\frac{Kk_{ro}}{\mu_o}\frac{1}{1 + \frac{k_{ro}}{k_{rw}}\frac{\mu_w}{\mu_o}}\frac{dP_c}{dS_w} \tag{14}$$

D is a non-linear function of water saturation. We define the normalized water saturation as below:

$$S = f(x,y,z,t) = \frac{S_w - S_{wi}}{1 - S_{or} - S_{wi}} \tag{15}$$

So, S is the ratio of recovered oil to the total recoverable oil. By inserting the parameter S, Eq. (13) converts into the following correlation:

$$\varphi\frac{\partial(S)}{\partial t} + \frac{\partial}{\partial x}\left(D.\frac{\partial S}{\partial x}\right) + \frac{\Delta\rho.g_x}{1 - S_{wi} - S_{or}}.\frac{\partial}{\partial S}\left(\frac{k_w k_o}{k_o\mu_w + k_w\mu_o}\right).\frac{\partial S}{\partial x} + \frac{\partial}{\partial y}\left(D.\frac{\partial S}{\partial y}\right) + \frac{\Delta\rho.g_y}{1 - S_{wi} - S_{or}}.\frac{\partial}{\partial S}\left(\frac{k_w k_o}{k_o\mu_w + k_w\mu_o}\right).\frac{\partial S}{\partial y} + \frac{\partial}{\partial z}\left(D.\frac{\partial S}{\partial z}\right) + \frac{\Delta\rho.g_z}{1 - S_{wi} - S_{or}}.\frac{\partial}{\partial S}\left(\frac{k_w k_o}{k_o\mu_w + k_w\mu_o}\right).\frac{\partial S}{\partial z} = 0 \tag{16}$$

In order to investigate the effect of gravity, a cube core has been modeled in z direction (Fig.2), in this state, all surfaces except one are impermeable. So, Eq. (16) converts into the following correlation:

$$\varphi\frac{\partial(S)}{\partial t} + \frac{\partial}{\partial z}\left(D.\frac{\partial S}{\partial z}\right) + \frac{\Delta\rho.g_z}{1 - S_{wi} - S_{or}}.\frac{\partial}{\partial S}\left(\frac{k_w k_o}{k_o\mu_w + k_w\mu_o}\right).\frac{\partial S}{\partial z} = 0 \tag{17}$$

Eq. (17) is discretized as following:

$$S(i,j,k)^{n+1} - S(i,j,k)^n + \frac{Di,j,k+\frac{1}{2}.\Delta t}{\varphi.h^2}.S(i,j,k+1)^{n+1} - \frac{Di,j,k+1/2\,.\Delta t}{\varphi.h^2}.S(i,j,k)^{n+1} + \frac{Di,j,k-1/2\,.\Delta t}{\varphi.h^2}.S(i,j,k-1)^{n+1} - \frac{Di,j,k-1/2\,.\Delta t}{\varphi.h^2}.S(i,j,k)^{n+1} + \frac{\Delta t}{\varphi.2h}.\frac{\Delta\rho.g_z}{1 - S_{wi} - S_{or}}.\frac{\partial}{\partial S}\left(\frac{k_w k_o}{k_o\mu_w + k_w\mu_o}\right).S(i,j,k+1)^{n+1} - \frac{\Delta t}{\varphi.2h}.\frac{\Delta\rho.g_z}{1 - S_{wi} - S_{or}}.\frac{\partial}{\partial S}\left(\frac{k_w k_o}{k_o\mu_w + k_w\mu_o}\right).S(i,j,k-1)^{n+1} = 0 \tag{18}$$

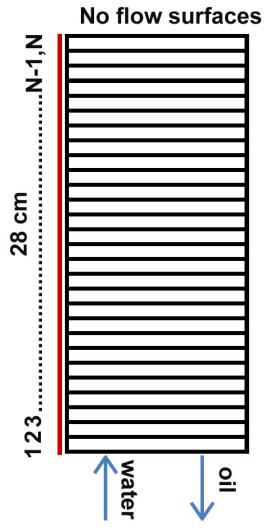

Figure. 2 Grid geometry for 1D

u_{wx} u_{wz} The superscript indicates the time level. n is the old time level for which we have a complete solution and all variables and properties. n+1 is the new time level and variables and properties are unknown. Eq. (18) is valid for the internal blocks.

At the permeable surfaces in contact with water, boundary conditions are set to be S_w=1 - S_{or}, the blocks of impermeable surfaces are unknown so the mass balance must be written for impermeable surfaces. Initial conditions are equal to initial water saturation, so S=0.

At the impermeable surface (In node number N), mass equation is given as below:

$$\frac{\frac{2k_w k_o}{k_o\mu_w + k_w\mu_o}(g(\rho_w - \rho_o) + \frac{\partial Pc}{\partial S_w}.\frac{\partial S_w}{\partial z})}{dz} = \varphi\frac{\partial S_w}{\partial t} \quad (19)$$

Eq. (19) is discretized as below:

$$\frac{2k_w k_o g(\rho_w - \rho_o)}{(k_o\mu_w + k_w\mu_o)h_z.(1 - S_{wi} - S_{or})} + \frac{2D}{h_z}.\frac{S(i,J,N)^{n+1} - S(i,j,N-1)^{n+1}}{h_z} = \varphi.\frac{S(i,j,N)^{n+1} - S(i,j,N)^{n}}{\Delta t} \quad (20)$$

Finally, there are (N-1) equations for (N-1) unknown nodes that must be solved simultaneously.

If the matrix is very low hydrophilic or the core is too high, the capillary pressure has low effect on imbibition process. In this section, a mathematical formulation of the imbibition is presented, that the capillary terms are neglected. Water and oil velocity in z direction can be obtained using Darcy's law, so following equations will be obtained:

$$u_{wz} = \frac{K.k_{rw}}{\mu_w}\left(-\frac{\partial P_{wo}}{\partial z} - \rho_w g_z\right) \quad (21)$$

$$u_{oz} = \frac{K.k_{ro}}{\mu_o}\left(-\frac{\partial P_{wo}}{\partial z} - \rho_o g_z\right) \quad (22)$$

$$\frac{\partial P_w}{\partial z} = -\frac{\mu_w U_{wz}}{Kk_{rw}} - \rho_w g_z \quad (23)$$

$$\frac{\partial P_o}{\partial z} = -\frac{\mu_o U_{oz}}{Kk_{ro}} - \rho_o g_z \quad (24)$$

$$\frac{\partial P_c}{\partial z} = \frac{\partial(P_o - P_w)}{\partial z} = \frac{\mu_w u_{wz}}{Kk_{rw}} - \frac{\mu_o u_{oz}}{Kk_{ro}} - \Delta\rho g_z \quad (25)$$

$$\frac{\partial P_c}{\partial z} = 0 \quad (26)$$

$$u_{oz} = -u_{wz} \quad (27)$$

$$u_{wz} = \Delta\rho.g.K\left(\frac{k_{ro}k_{rw}}{k_{ro}\mu_w + k_{rw}\mu_o}\right) \quad (28)$$

by inserting Eq. (28) into Eq. (1), the governing equation will be obtained as follows:

$$\varphi\frac{\partial S}{\partial t} + \frac{\partial}{\partial S_w}\left(\Delta\rho.g_z.K\frac{k_{ro}k_{rw}}{k_{ro}\mu_w + k_{rw}\mu_o}\right)\frac{\partial S}{\partial z} = 0 \quad (29)$$

Eq. (29) is discretized as below:

$$\frac{S(i,j,k)^{n+1} - S(i,j,k)^{n}}{\Delta t} + \frac{\partial}{\partial S_w}\left(\Delta\rho.g_z.K\frac{k_{ro}k_{rw}}{k_{ro}\mu_w + k_{rw}\mu_o}\right), \frac{S(i,j,k+1)^{n+1} - S(i,j,k-1)^{n+1}}{2h_z} = 0 \quad (30)$$

Equation (30) is valid for the internal blocks. In node number N, the mass equation must be written again, mass equation is given as below:

$$\frac{\frac{2k_w k_o}{k_o\mu_w + k_w\mu_o}(g(\rho_w - \rho_o)}{dz(1 - S_{or} - S_{wi})} = \varphi\frac{\partial S}{\partial t} \quad (31)$$

eq. (31) is discretized as below:

$$\frac{\frac{2k_w k_o}{k_o\mu_w + k_w\mu_o}(g(\rho_w - \rho_o)}{dz(1 - S_{or} - S_{wi})} = \varphi\frac{S(i,j,N)^{n+1} - S(i,j,N)^{n}}{\Delta t} \quad (32)$$

Finally, there are (N-1) equations for (N-1) unknown nodes. These equations must be solved simultaneously. MATLAB program is used to simulate, and fig.3 shows the modeling results.

3. RESULTS AND DISCUSSION

In order to investigate the sensitivity of gravity on counter-current imbibition rate, the vertical cube core was modeled by finite difference method and using MATLAB program.

The numerical results are compared with the experimental data of oil recovery and simulation results by Eclipse®-100, in Fig.3 to examine the validity of the proposed method [2, 5].

Fig.3 shows that numerical and experimental results are consistent, except at the end times. The capillary or gravity forces can act as dominant force to control the imbibition rate.

According to the matrix property and the position of the matrix and the fracture, the dominant force is determined. In the most position the capillary forces are driving force and the gravity effect can be neglected. Fig.3 and 4 show oil recovery as a function of time for three different positions that driving force is only capillary force, only gravity force or both of them. Fig.3 shows oil recovery in a core with low height, h=0.28m, here driving force is capillary pressure and gravity force has no significant effect.

Fig.4 shows oil recovery in a core with h=3.0 m, in this height, the effect of gravity is significant, also, the effect of gravity is more than capillary effects and both of them are driving force. So, increasing the height of core will increase the effect of gravity and decrease the effect of capillary forces. Neglecting the gravity force will cause a lot of error in predicting the oil recovery by imbibition process from high reservoirs.

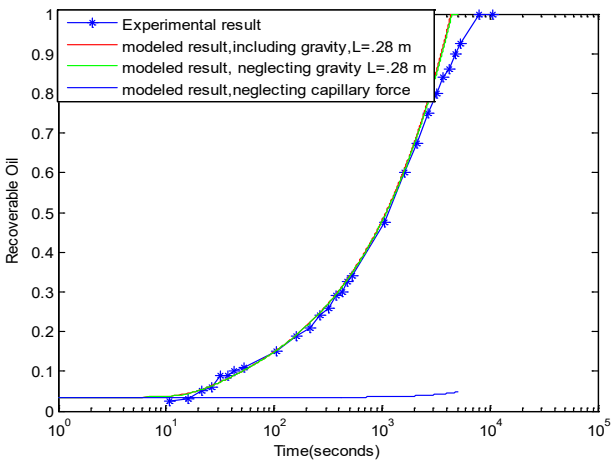

Figure. 3 Comparison of experimental and simulated results for three different positions that driving force is only capillary force, only gravity force or both of them, the core height=0.28m. The experimental data is from Bourbiaux et al. [5] and Behbahani et al. [2].

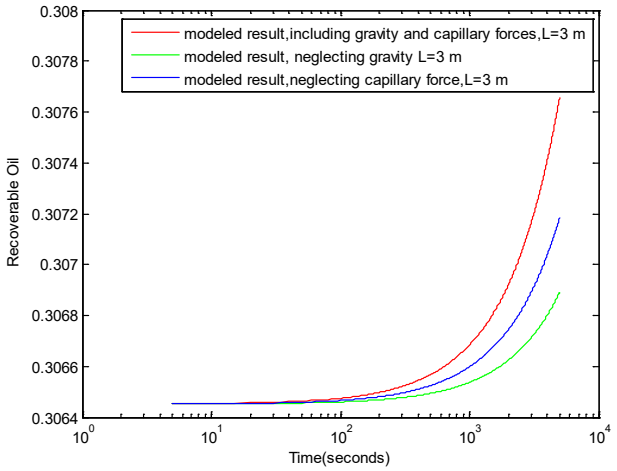

Figure. 4 Comparison of oil recovery as a function of time for three different positions that driving force is only capillary force, only gravity force or both of them, the core height=3m.

4. CONCLUSIONS

- The oil recovery mechanism during imbibition in cube core has been analyzed using the conservation mass and auxiliary equations.
- The capillary force is driving force of imbibing the water into the matrix block with low height.
- The effect of gravity force is significant for oil recovery from high matrix.
- Increasing the height of core will increase the effect of gravity and decrease the effect of capillary forces.

5. NOMENCLATURE

CDC : Capillary diffusivity coefficient

D : Capillary diffusion coefficient [m^2/s]

H : fluid [oil or water]

i : Integer denoting cell location in x-directions

j : Integer denoting cell location in y-directions

k : Integer denoting cell location in z-directions

K : Absolute permeability [darcy or m^2]

k_h : Effective permeability to fluid h [darcy or m^2]

k_{ro} : Relative permeability to oil

k_{rw} : Relative permeability to water

n : Integer indicating time level

N : Total number of nodes

P_C : Capillary pressure [Pa]

P_h : fluid h (oil or water) pressure [Pa]

P_o : Oil pressure [Pa]

P_w : Water pressure [Pa]

S : Normalized water saturation [fraction, m^3/m^3]

S_{Ai} : Distance from the open surface to the center of the matrix [m]

S_o : Oil saturation at time t in position (r,z) [fraction,m^3/m^3]

S_{or} : Residual oil saturation in the matrix [fraction, m^3/m^3]

S_w : Water saturation at time t in position (r,z) [fraction,m^3/m^3]

S_{wi} : Initial water saturation in the matrix [fraction,m^3/m^3]

T : Imbibition time [s]

u_{hx} : Fluidh (oil or water) velocity in x-direction [m/s]

u_{ox} : Oil velocity in x-direction [m/s]

u_{oy} : Oil velocity in y-direction (m/s)

u_{oz} : Oil velocity in z-direction [m/s]

u_t : Total velocity [m/s]

u_{wx} : Water velocity in x direction [m/s]

u_{wy} : Water velocity in y direction [m/s]

u_{wz} : Water velocity in z direction [m/s]

V : Volume of the matrix [m^3]

x : Coordinate in x-direction

y : Coordinate in y-direction

z : Coordinate in z-direction

μ_h : Fluid h viscosity [Pa.s]

μ_o : Oil viscosity [Pa.s]

μ_w : Water viscosity [Pa.s]

REFERENCES

1. R. P. Kinjal, N. M. Manjo, R. P. Twinkle, "A Mathematical Model of Imbibition Phenomenon in Heterogeneous Porous Media during Secondary Oil Recovery Process" Applied Mathematical Modelling, Vol.37, pp. 2933-2942 (2012).

2. H. Sh. Behbahani, G. Di Donato, M. J. Blunt, "Simulation of counter-current imbibition in water-wet fractured reservoirs" Journal of Petroleum Science and Engineering, Vol. 50, pp.21-39 (2005).

3. P. M. Blair, Humble Oil and Refining Co. "Calculation of Oil Displacement by Countercurrent Water Imbibition" SPE Journal 873-PA, Vol. 4, No. 3, pp. 195-202 (1964).

4. B. L. Beckner, K. Ishimoto, S. Yamaguchi, A. Firoozabadi, K. Azis, "Imbibition-Dominated Matrix-Fracture Fluid Transfer in Dual Porosity Simulators" presented at the SPE Annual Technical Conference and Exhibition, Dallas, Texas (1987).

5. B. J. Bourbiaux, F. J. Kalaydjian, "Experimental study of concurrent and countercurrent flows in natural porous media" SPE Reserv. Eng., Vol.5, pp. 361- 368 (1990).

Impact of Compressor Performance on the Flow Capacity of Gas Transmission Pipelines

• **Seyed Mohammad Fatemi[1], Morteza Esfandyari[2*], Mahdi Koolivand- Salooki[3]**
1. Petroleum Department, National Iranian South Oilfield company, Ahvaz, Iran
2. Department of Chemical Engineering, University of Bojnord, Bojnord, Iran
3. Gas Research Division, Research Institute of Petroleum Industry, Tehran, Iran
Corresponding author Email address: M.Esfandyari@ub.ac.ir

Received: Feb. 14, 2017 / Accepted: May. 01, 2017

Abstract

Flow capacity of a gas transmission pipeline is usually affected by different parameters. In this study several determining factor are selected for sensitivity analysis of flow capacity prediction in IGAT-IV. These parameters include; pipeline parameters, gas parameters, system parameters, heat transfer parameters, compression parameters and compressor fuel consumption parameters. Detail calculation has been performed by developing a computer program by Microsoft Visual Basic. Moreover, a computer program for generating the compressor performance curve has been written by MATLAB. This curve has been used to design and optimize the compressor stations. From the present investigation, it has concluded that AGA Fully Turbulent, Colebrook-White and Weymouth equations have the best prediction of flow rate in gas transmission pipelines. 87.85 % flow changes due to 1% isentropic exponent change, which has a very large effect on the flow capacity. 10% to 30% flow changes due to 1% suction compressibility factor and discharge compressibility factor change. They have large effect on the flow capacity. 1% to 10% flow changes due to 1% compressor horsepower, compressor suction and discharge temperature and adiabatic efficiency change. They have medium effect on the flow capacity. The other parameters have not significant effect on the flow capacity.

Keywords: Gas Transmission Pipeline, Flow Capacity, Compression parameters, Compressor Fuel Consumption Parameters.

1. Introduction

Oil and gas are the most important sources of energy in the world. They have prepared about 90% of total energy that is used in industries, homes etc. Modern people's lives are based on an environment in which energy plays a main role. Oil and gas are major participants in the study of energy, and pipelines are the primary means by which they are transport. These pipelines are mostly buried and operate without distributing normal pursuits. They carry large volume of natural gas, crude oil, and other products in continuous streams.

During the last 60 years, the transportation of natural gas from wells to city distribution systems has developed from a single low-pressure line 25 miles long, made of short lengths of 8-inch diameter wooden pipe, to one of the most important branches of the petroleum and natural gas industry. Thousands of miles of large diameter steel pipe are carrying natural gas between the sources of supply and points of consumption[1, 2]

Gas (or any Newtonian fluid) will flow through a pipe as long as there is a pressure differential between the inlet and outlet of the pipe. For natural gas pipeline systems, two main forces affect the movement of the gas from one point to another: frictional and gravitational forces. These frictional and gravitational forces reduce the pressure (or energy) of the gas as it moves down the pipe. In order to maintain flow in the pipe, there must be a counteracting force (or energy) to overcome these frictional and gravitational forces and still maintain a pressure differential between any point in the pipe and the terminal point and ultimately meet the delivery requirements of the downstream customer[1-4].

Demissie and Zhu [5] in 2015, conducted a literature survey of pipeline design and pipeline operations. Ríos-Mercado and Borraz-Sánchez [6] in 2015 conducted a literature survey on line-pack, pooling, and fuel cost minimization problems. Demissie el al.[7] In 2017 proposed models for gas pipeline operation, then they have optimized these models. These models are optimized for different structures of the gas pipeline network. Optimization of these models was done using NSGA-II algorithm. Chaczykowskia, and Zarodkiewicz [8] in 2017 Simulated the distribution of natural gas quality for pipeline systems. The results of this model show that gas quality has a significant impact on pipeline inventory and pipeline capacity of the pipeline system.

In the gas industry, the compressor frequently provides this counteracting force or pressure boost. Two types of compressors are used widely in the industry: reciprocating and centrifugal compressors. The reciprocating units boost (or increase) the gas pressure by a direct reduction of the gas volume through the displacement action of its pistons (Boyle's law). The centrifugal units, on the other hand, increase gas pressure by the dual process of radial acceleration of the gas by rotating impellers and velocity reduction by stationary diffusers (i.e., conversion of velocity to head or pressure).The horsepower and the changing compression ratio and the variation of adiabatic efficiency and the ambient temperature and the heat rate/constant and the isentropic exponent were the heat transfer parameters that were analyzed.

This study is the product of questions raised from various groups and individuals within National Iranian Gas Company (and indeed in the rest of the industry) with respect to the significance of various parameters and criteria on the planning and design of pipeline facilities. An attempt is made here to quantify the impact of "reasonable" variations in each parameter or criteria separately. "Reasonable" variations imply possible variations in the design parameters criteria that are likely to affect the physical state, performance and cost or service of the pipeline system during its projected service life. Such variations may occur due to seasonal changes (e.g. ambient temperature, thermal conductivity), age and service (e.g. roughness, compressor, and pipe deration), changes in the physical state and conditions of the pipeline system (e.g. new pipe/ compression facilities, gas composition, terrain, etc.), or perhaps changes in business and regulatory environment (e.g. rate of return, interest rates, etc.)

2. Gas transmission methods

Gas is difficult to store because of its physical nature and needs high pressures and/or low temperatures to increase the bulk density. It needs to be transported immediately to its destination after production from a reservoir. There are a number of methods of exporting gas energy from an isolated field for use elsewhere. The methods include: Pipelined Natural Gas(PNG), Liquefied Natural Gas (LNG), Gas to Liquids (GTL), Gas to Commodity (GTC), Gas to Wire (GTW), Compressed Natural Gas (CNG), Gas to Solids (GTS)[9, 10].

3. Gas physical properties prediction

The physical properties of a natural gas may be obtained directly either by laboratory measurements or by prediction from the known chemical composition of the gas. In the latter case, the calculations are based on the physical properties of individual components of the gas and upon physical laws, often referred to as mixing rules, relating the properties of the components to those of the gas mixture. For gas compressibility, factor calculation used Standing-Katz chart that curve-fitted by Gopal. For calculation of pseudo critical pressure and temperature and apparent molecular weight and heat capacity of gas mixtures used kay's rules. For calculation of gas thermodynamic properties and density of gas mixtures used real gas laws. For calculation of gas viscosity used Lee-Gonzales-Eakin method [11-15].

4.Flow equations and correlations for gas compressors

4.1.Adiabatic work gas compression

The pressure-volume relationship in an adiabatic process is defined as $P.V^k = cte$, to calculate the work required to compress a gas adiabatically we have this relation[14]:

$$-W = \int_1^2 V.dP \tag{1}$$

Substituting for V

$$-W = \int_1^2 cte^{1/k}.P^{1/k}.dP$$

Moreover, after integration and further simplification in Imperial Units:

$$-W = \frac{53.28}{G}.T_1.\frac{k}{k-1}.\left[\left(\frac{P_2}{P_1}\right)^{\frac{k-1}{k}} - 1\right] \tag{2}$$

Where $-W$ is a Work (head) to be done on the compressor to adiabatically compress gas from P_1 to P_1 $(ft.lb_f / lb_m)$, G is a gas gravity, dimensionless, T_1 is a suction temperature,$(°R)$, k is an adiabatic gas exponent, dimensionless, P_1 is a suction pressure, psia, P_2 is a discharge pressure, psia and P_2/P_1 is a compression ratio (CR), dimensionless.

4.2.Temperature change in adiabatic gas compression

In adiabatic gas compression, gas temperature increases according to the equations described below[15].

$$\frac{Z_2.T_2}{Z_1.T_1} = \left(\frac{P_2}{P_1}\right)^{\frac{k-1}{k}} \tag{3}$$

4.3.Compressor head and horsepowern

Head is the amount of work or energy injected into the gas to raise its pressure from P_1 to P_2 . It has the units of kJ/kg in SI or $ft.lb_f / lb_m$ in imperial units. On the other hand, horsepower (HP) is defined as[15]:

$$HP = \frac{MassFlow\ .\ Head}{Thermal\ Efficiency\ of\ Compression} \tag{4}$$

With some assumption and simplification [1], we have:

$$HP = 0.0857.\frac{k}{k-1}.T_1.\frac{Z_1+Z_2}{2}.\frac{1}{\eta_a}.\left[\left(\frac{P_2}{P_1}\right)^{\frac{k-1}{k}} - 1\right] \tag{5}$$

Where HP is an adiabatic power requirement, (HP/l MMSCFD), T_1 is a suction temperature, ($°R$) , P_1 is an adiabatic gas exponent, dimensionless, is a suction pressure, psia, P_2 is a discharge pressure, psia and P_2/P_1 is a compression ratio (CR), dimensionless and η_a is an adiabatic (isentropic) efficiency, which is typically in the range of 0.75 to 0.79.

4.4.Adiabatic (isentropic) efficiency

Adiabatic (isentropic) efficiency η_a is defined as the ratio between adiabatic (isentropic) head and the actual head as follows[14]:

$$\eta_a = \frac{(Head)_{adiabatic}}{(Head)_{actual}} \tag{6}$$

Adiabatic (isentropic) efficiency of a gas compressor could also be represented by the following equation[15]:

$$\eta_a = \frac{T_1\left[\left(\frac{P_2}{P_1}\right)^{\frac{k-1}{k}} - 1\right]}{T_2 - T_1} \tag{7}$$

k is normally determined at the average of suction and discharge temperatures.

4.5. Horsepower and gas flow

From section 4.3 we have following relation:

$$HP = 0.0857.\frac{k}{k-1}.T_1.\frac{Z_1+Z_2}{2}.\frac{1}{\eta_a}.\left[\left(\frac{P_2}{P_1}\right)^{\frac{k-1}{k}} - 1\right] \tag{8}$$

Where HP = adiabatic power requirement, (HP/l MMSCFD). So we can rewrite the relation in the following form:

$$\frac{HP}{Q} = 0.0857.\frac{k}{k-1}.T_1.\frac{Z_1+Z_2}{2}.\frac{1}{\eta_a}.\left[\left(\frac{P_2}{P_1}\right)^{\frac{k-1}{k}} - 1\right] \tag{9}$$

$$Q = \frac{HP}{0.0857.\frac{k}{k-1}.T_1.\frac{Z_1+Z_2}{2}.\frac{1}{\eta_a}.\left[\left(\frac{P_2}{P_1}\right)^{\frac{k-1}{k}} - 1\right]} \tag{10}$$

4.6.Compressor available power

The compressor power, available at pressure and temperature of site condition is calculated as follows:

$$HP_{site} = HP_{ISO}.F_p.F_t \tag{11}$$

Where HP_{site} is a site available power (HP), HP_{ISO} is a sea level (ISO) power (HP), F_p is a site elevation adjustment factor and F_t is an ambient temperature adjustment factor.

4.7.Compressor fuel consumption

The fuel consumption of compressors is calculated by flowing methods:

1. Use heat rate curve of compressor and following formula:

$$fuel = Heat\ Rate, HP \tag{12}$$

Where $fuel$ is a fuel consumption (kJ/h), $Heat\ Rate$ is a heat rate (kJ/kWh) and HP is compressor power (kW). For the relationship between fuel and power, generally we have a curve or correlation, which shows the heat rate as a function of temperature and speed. With the known speed and power, the heat rate will be defined. Generally the standard curves have been generated at 15 $^{\circ}C$. In order to convert to another temperature the following correction factor will be used.

$$Correction\ Factor = \sqrt{\frac{273.15 + T_{amb}}{288.15}}.(0.9895 + 0.0007\ T_{amb} \tag{13}$$

Where T_{amb} is ambient temperature $^{\circ}C$.

2. Use the following formula:

$$fuel = A_f + B_f.HP \tag{14}$$

Where is $fuel$ consumption (kJ/h), A_f is a fuel gas constant (ft^3/day) and B_f is fuel gas rate constant ($ft^3/day.HP$)

The fuel coefficients are related to the compressor heat rate coefficient as follows:

$$A_f = 24\frac{A_H}{LHV} \tag{15}$$

$$B_f = 24\frac{B_H}{LHV} \quad (16)$$

Where A_H is heat constant (BTU/hr) , B_H is a heat rate constant (BTU/hr.HP) and LHV is lower heating value.

Therefore, the fuel gas flow is calculated as follows:

$$Fuel\ Gas\ Flow = \frac{fuel}{24 \times LHV \times \eta_T} \quad (17)$$

Where η_T is turbine efficiency.

5.Impact of different parameters on the hydraulic and flow capacity of gas transmission pipelines

The parameters that affect flow capacity of gas transmission pipelines are:

1.Compressor parameters

The compressor parameters are essentially those parameters, which affect the fuel consumption and therefore flow behavior of the gas during transmission. The compressor parameters are shown in Table. 1.

Table. 1: Compression parameters

Items	Parameter
1	Suction pressure
2	Discharge pressure
3	Compression ratio
4	Suction temperature
5	Discharge temperature
6	Suction compressibility factor
7	Discharge compressibility factor
8	Adiabatic efficiency
9	Isentropic exponent
10	Horse power

2.Compressor fuel consumption parameters

The compressor fuel consumption parameters are essentially those parameters, which affect the compressor fuel consumption. These parameters are shown in Table. 2.

Table. 2: Compressor fuel consumption parameters

1	Ambient temperature adjustment factor
2	Site elevation adjustment factor
3	Gas lower heating value.
4	Heat rate curve
5	RPM of compressor
6	Turbine efficiency
7	Compressor performance curve(wheel map)

6.Case Study

For the sensivity analysis, we choose the special part of IGAT-IV pipeline that has maximum change in parameters. Therefore, we choose the following part of IGAT-IV for sensivity analysis with properties that shown in Table.3 and Table.4

Table. 3: Compression parameter for compressor#6 of IGAT IV pipeline

Compression Parameters	Value
Suction pressure(psia)	947.52
Discharge pressure(psia)	1319.7
Compression patio(Pout/Pin)	1.39
Suction temperature(R)	549.66
Discharge temperature(R)	605.62
Suction compressibility factor	0.87
Discharge compressibility factor	0.89
Adiabatic efficiency	0.75
Isentropic exponent(Kin+Kout)/2	1.51
Horse power(hp)	73727.11

Table. 4: Gas composition of refinery outlet

Gas Composition	Mole Percent	Gas Composition	Mole Percent
Methane	0.9	n-Hexane	2.00E-04
Ethane	5.00E-02	n-Heptanes	2.00E-04
Propane	6.00E-03	Nitrogen	3.20E-02
n-Butane	1.00E-03	CO_2	1.00E-02
n-Pentane	6.00E-04	-	-

7.Sensitivity Results

The data from IGATIV pipeline were introduced to the written program by Microsoft visual basic. At first the physical properties of gas calculated. Then sensitivity analysis for each parameter. The sensitivity results from generated program are shown in the following figures.

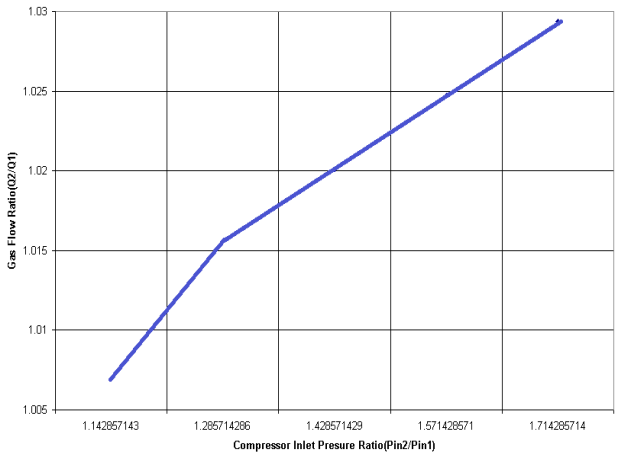

Figure 1. The impact of compressor suction pressure ratio on gas flow ratio

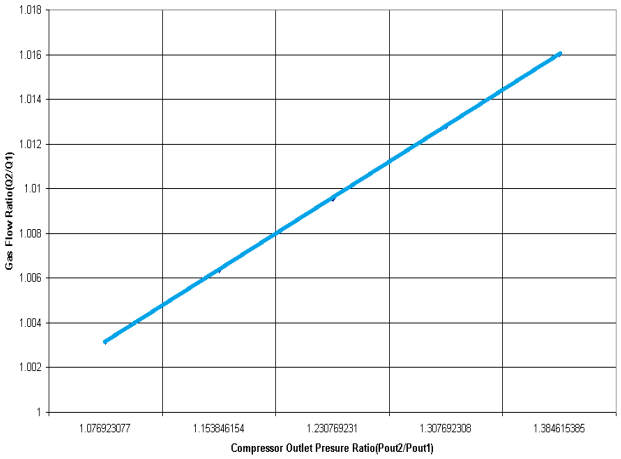

Figure 2. The impact of compressor discharge pressure ratio on gas flow ratio

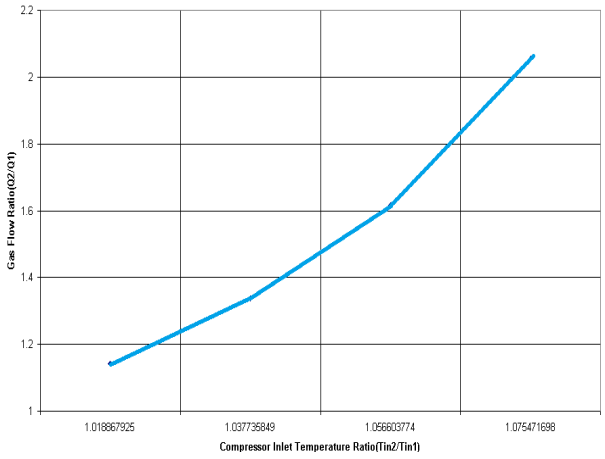

Figure 3. The impact of compressor suction temperature ratio change on gas flow ratio

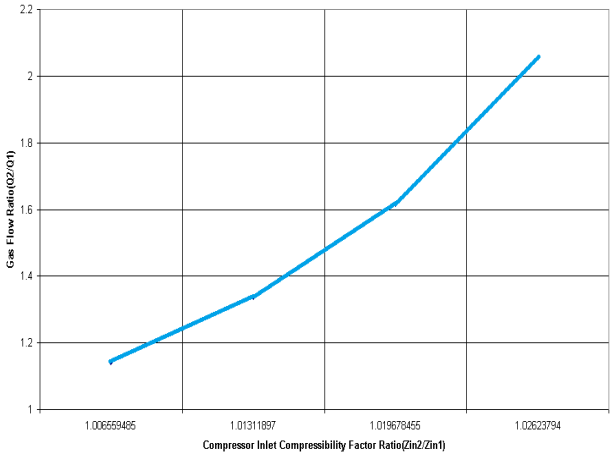

Figure 4. The impact of gas suction compressibility factor ratio change on gas flow ratio

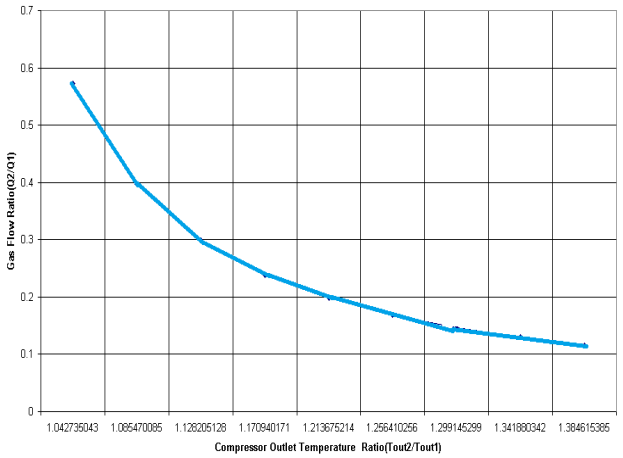

Figure 5. The impact of compressor gas discharge temperature ratio change on gas flow ratio

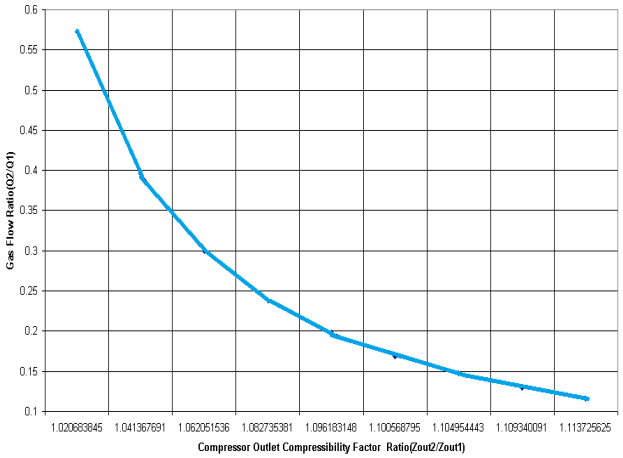

Figure 6. The impact of compressor discharge compressibility factor ratio change on gas flow ratio

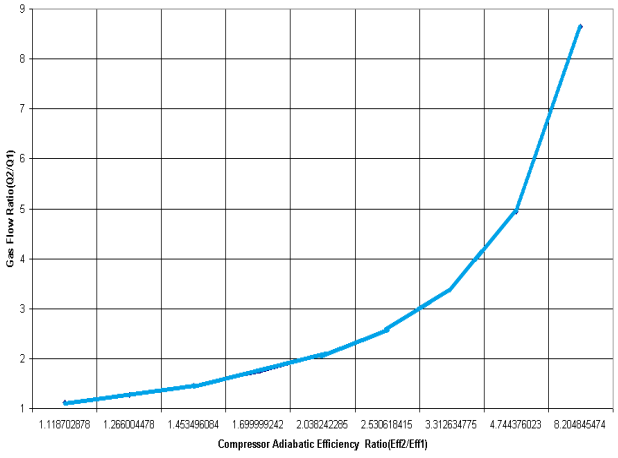

Figure 7. The impact of compressor adiabatic efficiency ratio change on gas flow ratio

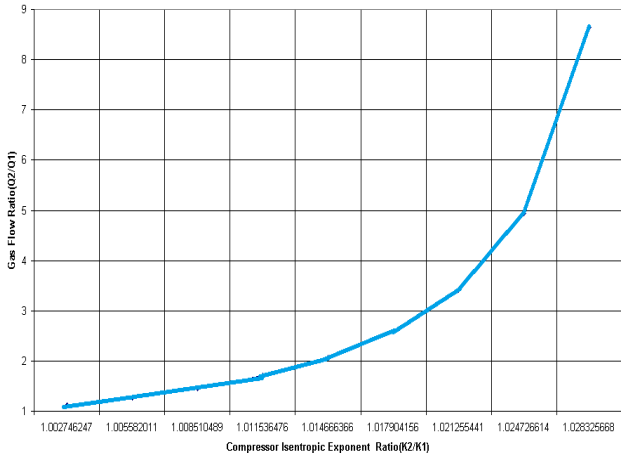

Figure 8. The impact of compressor isentropic exponent ratio change on gas flow ratio

8.Results

The main objective of this work was to investigate the impact of different parameters on the hydraulic and flow capacity of a gas transmission pipelines. To achieve these objectives, the impact of gas compression parameters and compressor fuel consumption parameters on the physical properties of gases was firstly studied. The result of this study were introduced into general flow equation of gas transmission pipelines and compression equations, for estimating the effect of these changes on the hydraulic and flow capacity of pipelines. From the present investigation, the following results are concluded:

- All of commercial software's get the flow as an input data, therefore they cannot easily used for sensitivity analysis on flow.
- The fuels of compressor stations are taken from the transmission pipelines. Therefore, it is too important to optimize the compressor performance. For this reason, we should use compressor performance curve.
- If horse power, suction pressure, discharge pressure, compression ratio, suction temperature, suction compressibility factor, adiabatic efficiency, isentropic exponent, turbine efficiency, gas lower heating value increases the flow capacity increases.
- If discharge temperature, discharge compressibility factor, ambient temperature adjustment factor, site elevation adjustment factor, heat rate curve increases the flow capacity decreases.
- 87.8578% flow changes due to 1% isentropic exponent change. It has a very large effect

on the flow capacity.

- 10% to 30% flow changes due to 1% suction compressibility factor, discharge compressibility factor change. They have large effect on the flow capacity.
- 1% to 10% flow changes due to 1% compressor horse power, compressor suction and discharge temperature and adiabatic efficiency change. They have medium effect on the flow capacity.
- 0% to 0.1% flow changes due to 1% compressor suction and discharge pressure, compressor compression ratio change. They have very small effect on the flow capacity.
- If ambient temperature increases (decreases), the air mass flow rate decreases (or increases) and the power output of the compressor decreases (or increases) .Therefore fuel consumption of compressor increases and then fuel gas flow increases. Increase in fuel gas flow means decrease in gas flow of pipeline.
- If site elevation increases (or decreases), the air mass flow rate decreases (or increases) and the power output of the compressor decreases (or increases). Therefore fuel consumption of compressor increases and then fuel gas flow increases. Increase in fuel gas flow means decrease in gas flow of pipeline.
- If turbine efficiency increases the fuel, gas flow decreases. Decrease in fuel gas flow means increase in gas flow of pipeline.
- If gas lower heat capacity increases, the fuel gas flow decreases. Decrease in fuel gas flow means increase in gas flow of pipeline.
- If heat rate increases the fuel of the compressor increases. Therefore, fuel gas flow increases. Increase in fuel gas flow means decrease in gas flow of pipeline.
- The heat rate curve is usually plot for different RPM of compressor with experimental data. Therefore, the effect of RPM is dependent on heat rate curve.
- Results that are more detailed are shown in below tables.

Table. 5: Summary of Results, Design Criteria and Parameters Impact Study

Compression Parameters	Variation in Parameter	Change in Flow (MMSCFD)	Remarks
Horse power	---------- increase	---------- increase	$Q = Gas\ Compressor\ Parameters \times HP_t$ $GCP = \frac{1}{0.0857.\frac{k}{k-1}.T_s.\frac{Z_s+Z_d}{2}.\frac{1}{\eta_a}.\left[\left(\frac{P_d}{P_s}\right)^{\frac{k-1}{k}}-1\right]}$
	1% flow change for 1% parameter chang		
Suction Pressure	700 psia<Ps<1200 psia Stepsize=100 psia Change=14.28% increase	3788.967<Q<3900.19 Average change per stepsize=0.587% increase	Suction compressibility factor, Adiabatic efficiency, Compression ratio are change due to change of Suction Pressure
	0.04110% flow change for 1% parameter change		
Discharge Pressure	1300 psia<Pd<1800 psia Stepsize=100 psia Change=7.6923% increase	3853.769<Q<3915.498 Average change per stepsize=0.3173% increase	Suction compressibility factor, Adiabatic efficiency, Compression ratio are change due to change of Suction Pressure
	0.04112% flow change for 1% parameter change		
Compression ratio	1.372<CR<1.899 Change=7.6922% increase	3853.769<Q<3915.498 Average change per stepsize=0.3173% increase	CR change due to change of Suction and Discharge pressure of compressor
	0.0412% flow change for 1% parameter change		
Suction Temperature	530 R<Ts<570 R Stepsize=10 R Change=1.8867% increase	2899.797<Q<5959.408 Average change per stepsize=16.8781% increase	Suction compressibility factor, Isentropic exponent, Adiabatic efficiency are change due to change of Suction Temperature
	8.9454 flow change for 1% parameter change		

Table. 6: Summary of Results, Design Criteria and Parameters Impact Study

Compression Parameters	Variation in Parameter	Change in Flow (MMSCFD)	Remarks
Suction Compressibility Factor	0.8681<Zs<0.8908 Change=0.6559% increase	2899.797<Q<5959.408 Average change per stepsize=16.8781% increase	Suction compressibility factor change due to change of Suction temperature
	25.7323% flow change for 1% parameter change		
Discharge Temperature	585 R<Td<810 R Stepsize=25 R Change=4.2735% increase	6221.131>Q>720.1678 Average change per stepsize=30.2032% decrease	discharge compressibility factor, Isentropic exponent, Adiabatic efficiency are change due to change of Discharge Temperature
	0.04110% flow change for 1% parameter change		
Discharge Compressibility Factor	0.8754<Zd<0.9750 Change=2.0683% increase	6221.131>Q>720.1678 Average change per stepsize=30.2032% decrease	discharge compressibility factor change due to change of Discharge Temperature
	14.6028% flow change for 1% parameter change		
Adiabatic Efficiency	1.19<η_a<0.14 Change=23.3303% increase	6221.131>Q>720.1678 Average change per stepsize=30.2032% increase	Adiabatic efficiency is change due to change of Suction and Discharge Temperature, Isentropic Exponent and Suction and Discharge Pressure
	1.2945% flow change for 1% parameter change		
Isentropic Exponent	1.286<K<1.251 Change=0.3437% increase	6221.131>Q>720.1678 Average change per stepsize=30.2032% increase	Isentropic exponent change due to change of Discharge Temperature
	87.8578% flow change for 1% parameter change		

Table. 7: Summary of Results, Design Criteria and Parameters Impact Study

Compressor Fuel Consumption Parameters	Variation in Parameter	Change in Flow	Remarks
Ambient temperature adjustment factor	increase	decrease	$HP_{site} = HP_{ISO}.F_p.F_t$
Site elevation adjustment factor	increase	decrease	$HP_{site} = HP_{ISO}.F_p.F_t$
Heat Rate Curve	increase	decrease	$fuel = HeatRate.Hp$ $Q_{out} = Q_{in} - fuel$ $Q = Gas\ Compressor\ Parameters \times HP_t$
RPM of compressor	----------	----------	Depend on Heat Rate curve
Turbine Efficiency	increase	increase	$FuelGasFlow = \frac{fuel}{24 \times LHV \times \eta_T}$
Gas Lower Heating Value	increase	increase	

9.Conclusions

Main flow capacity parameters are selected in this study and their impact is investigated on one of the Iranian gas trunk line. These parameters includes pipeline variables, gas properties, system limitations, heat transfer factors, compressor variables and parameters. The results of sensitivity analysis are utilized by compression equations, for prognosticating of the selected factor effeteness on the gas pipelines flow capacity. In this study for making the calculation re a computer program is developed VB. Input data of developed program were selected from IGAT-IV pipeline data has been used as an inlet data for our developed program. This research highlighted that Fully Turbulent AGA, Colebrook-White and Weymouth equations predicts the flow rate of the gas transmission pipelines by a good accuracy.

Acknowledgment:

Author would like to appreciate national Iranian oil company (NIOC) and national Iranian south oil company (NISOC) for financial support of this study.

Nomenclature Symbol

P	Pressure (pisa)
P_1	suction pressure (psia)
P_2	discharge pressure (psia)
T	Temperature (°R)
T_1	suction temperature (°R)
T_2	discharge pressure (°R)
T_{amb}	ambient temperature (°C)
W	Work ($(ft.lb_f / lb_m)$)
G	gas gravity (-)
k	adiabatic gas exponent (-)
HP	compressor power (HP/l MMSCFD)
HP_{site}	site available power (HP)
HP_{ISO}	sea level (ISO) power (HP)
η_a	adiabatic (isentropic) efficiency (-)
Z	compressibility factor (-)
F_p	site elevation adjustment factor (-)
F_t	ambient temperature adjustment factor (-)
A_f	fuel gas constant (ft^3/day)
B_f	fuel gas rate constant(ft^3/day.HP)
A_H	heat constant (BTU/hr)
B_H	heat rate constant (BTU/hr.HP)
η_T	Turbine efficiency (-)

Abbreviation

PNG	Pipelined Natural Gas(-)
LNG	Liquefied Natural Gas (-)
GTL	Gas to Liquids (-)
GTC	Gas to Commodity (-)
GTW	Gas to Wire (-)
GTS	Gas to Solids (-)
HP	Horsepower (kW)
CR	compression ratio (-)
LHV	lower heating value(-)
VB	Visual Basic (-)

References

1. Mohitpour, M., H. Golshan, and A. Murray, Transient Flow in Liquid and Gas Pipelines. 2007: ASME press.
2. Tabkhi, F., et al., Improving the performance of natural gas pipeline networks fuel consumption minimization problems. AIChE journal, 2010. 56(4): p. 946-964.
3. Wong, P. and R. Larson, Optimization of natural-gas pipeline systems via dynamic

programming. IEEE Transactions on Automatic Control, 1968. 13(5): p. 475-481.

4. Yaqub, M. and S.M. Zubair, Performance evaluation of hot-gas by-pass capacity control schemes for refrigeration and air-conditioning systems. Energy, 2000. 25(6): p. 543-561.

5. Demissie, A. and W. Zhu. A Survey on Gas Pipelines Operation and Design Optimization. in IIE Annual Conference. Proceedings. 2015. Institute of Industrial and Systems Engineers (IISE).

6. Ríos-Mercado, R.Z. and C. Borraz-Sánchez, Optimization problems in natural gas transportation systems: A state-of-the-art review. Applied Energy, 2015. 147(Supplement C): p. 536-555.

7. Demissie, A., W. Zhu, and C.T. Belachew, A multi-objective optimization model for gas pipeline operations. Computers & Chemical Engineering, 2017. 100: p. 94-103.

8. Chaczykowski, M. and P. Zarodkiewicz, Simulation of natural gas quality distribution for pipeline systems. Energy, 2017.

9. Kumar, S., Gas production engineering. Vol. 4. 1987: Gulf Professional Publishing.

10. 10. Petroleum, I.o., Modern petroleum technology. 2000: Wiley.

11. McCain Jr, W., The properties of petroleum fluids: Penn Well Publ., 1984, Co.

12. Abbott, M.M., J.M. Smith, and H.C. Van Ness, Introduction to chemical engineering thermodynamics. McGraw-Hill, Boston, 2001: p. 619-626.

13. Association, G.P.S., Engineering data book. 1994: Gas Processor Supplier Association.

14. Danesh, A., PVT and phase behaviour of petroleum reservoir fluids. Vol. 47. 1998: Elsevier.

15. Mohitpour, M., H. Golshan, and A. Murray, Pipeline design and construction: A practical approach The American Society of Mechanical Engineers. Three Park Ave., New York, NY, 2007. 10016.

Pressure Drop in Randomly Packed Absorption Tower in Transient Flow Regime

• **Seyedeh Gita Sharafi, Rahbar Rahimi*, Morteza Zivdar**
1. Department of Chemical Engineering University of Sistan and Baluchestan, Zahedan, Iran
Corresponding author Email address: rahimi@hamoon.usb.ac.ir

Received: Oct. 28, 2017 / Accepted: Dec. 06, 2017

Abstract

In this work computational fluid dynamics is used to describe the fluid flow across a randomly packed absorption tower. The CFD simulation method is employed on a packed tower that is packed with 1cm Raschig rings. Tower is 175cm in height. Air flow rate range was 1.5 to 5 m/s. The measured pressure drops were in 1.5 to 12 Pascal per height of tower in meter. The Klerk's approach is examined to define the influence of confining walls on pressure drop in packed areas. It is concluded that CFD model that uses the Klerk's definition of radial porosity distribution is a successful way for pressure drop prediction in packed beds. Model prediction of dry pressure drop is about 4% lower than the experimental measurements. Ergun's pressure drop prediction is compared with that of Reichelt's using averaged and distributed porosity profiles. In both methods Ergun's approach in comparison with Reichelt's approach has %6 lesser error in dry pressure drop prediction.

Keywords: pressure drop, absorption packed tower, random packing, computational fluid dynamics.

1. INTRODUCTION

It is more than several decades that packed towers are widely used in chemical and petrochemical industries for gas absorption, distillation, and liquid-liquid extraction processes. In view of energy consumption pressure drop is an important parameter in packed tower design and selection of fluid flow equipment such as fans or blowers, compressors and pumps. Dry pressure drop is also an important design parameter in packed towers because it is required for wet pressure drop estimations and packing capacity evaluation [1].

Many pressure drop relations which are function of gas velocity and packed area properties are available in the literature [2-6]. The most famous one of them can be Ergun pressure drop relation for packed beds when just one phase flow through void spaces, which have been obtained experimentally [7]. Studies on the flow of Newtonian and non-Newtonian fluids through packed columns show the influence of confining walls on pressure drop prediction [8, 9]

Reichelt correlation [10] is one of the Ergun-type equations, which considered wall effect in pressure drop prediction equation by the terms A and B. Table 1 shows the pressure drop relations applied in this article. Eisfeld and Schnitzlein (2001) [11] compared the pressure drop correlations of Ergun's, Reichelt's, and the other approaches. Riechelt's approach was found more successful than others in small column diameter to packing diameter ratios (smaller than 10). Atmakidis and kenig (2009) [12] compared no-considering wall effect. Ergun's general approach with considering wall effect approaches such as Reichelt's in the CFD simulation of spherical packing in the packed bed with 1 and 7 column diameter to packing diameter ratios. Consideration of wall effects approaches were found more successful in pressure drop prediction than others in real geometry of packed bed simulation. In recent decades CFD is applied to solve complex calculations in packed towers. Numerical simulation solves engineering problems with an acceptable accuracy and reduces experimental costs, whilst makes available more local information which may not be attainable experimentally [13]. Packed towers simulation complexity is due to complex geometry of void spaces in randomly packed towers.

Two numerical approaches are applied to study transport phenomena in packed towers: first, considering exact geometry of packed bed which obtain by tomographic-based methods with high costs [12, 14]. In the second approach packed section is considered as porous media. Fluid flow governing equations and pressure drop correlations are applied to calculate fluid- solid interactions. Local phenomena is described as functions of radial and axial distribution of parameters [12]. Local voidage variation is one of the important parameters in simulation geometry description [15]. Most of the studies has resulted oscillatory damped behavior for radial porosity variation in packed sections [16, 17]. de Klerk [16] described radial porosity distribution by sinusoidal oscillatory damped function with exponential function near confining walls. Many researchers [18-23] applied second approach to model industrial packed towers with spherical and non-spherical packing such as Pall ring and Berl saddle in two dimensional (2D) and macro scale simulations. In this article, 3D CFD method in Eulerian-Eulerian frame is used to simulate a pilot scale tower that randomly packed with Raschig rings. Dry pressure drop is investigated

Table 1. Pressure drop predicting correlations

No.	Correlation	Constants	Wall effect correction	Ref.
1	$\frac{\Delta p}{Z} = 150\ \frac{(1-\varepsilon)^2\ \mu}{\varepsilon^3\ \left(D_p \emptyset_S\right)^2} U + 1.75 \frac{(1-\varepsilon)\rho_g}{\varepsilon^3 D_p \emptyset_S} U^2$	-	No	Ergun[7]
2	$\frac{\Delta p}{z} = \frac{154A^2}{Re}\frac{(1-\varepsilon)^2}{\varepsilon^3} + \frac{A}{B}\frac{(1-\varepsilon)}{\varepsilon^3}$	$A = 1 + \frac{2}{3\left(\frac{D}{dp}\right)(1-\varepsilon)}$ $B = \left[1.15\left(\frac{dp}{D}\right)^2 + 0.87\right]^2$	Yes	Reichelt [10]

In this study and validated experimentally. de Klerk's approach is applied to describe radial porosity distribution. Results has compared with simulation without wall effect consideration. In addition Ergun's approach is compared with Reichelt's approach in fluid flow resistance across the packed areas in tower diameter to packing effective diameter ratio approximately17.

2. Experimental procedure

Figure 1 shows experimental set-up used in this research. The column is 1.75m in height and 0.05m in diameter. The column has two separated packed sections. Each packed with approximately 1cm Raschig rings. Tower diameter to packing effective diameter ratio is about 17. Voidage measurements carried out by sudden stop of water supply and measured collected water volume. Air supplied at the bottom of column. Manometer was used for column pressure drop measurements along the column. Air flow measured by calibrated rotameter. Effective diameter of packing element is used to apply packing shape effect of non-spherical packed beds on pressure drop correlation [24]. Eq.3 and 4 show effective packing diameter, d_p , relations with sphericity factor, $\emptyset_S$, spherical equivalent diameter of packing, D_p and specific surface of a packing a_v.

$$a_v = \frac{Sp}{Vp} \tag{3}$$

$$d_p = D_p \emptyset_S = \frac{6}{a_v} \tag{4}$$

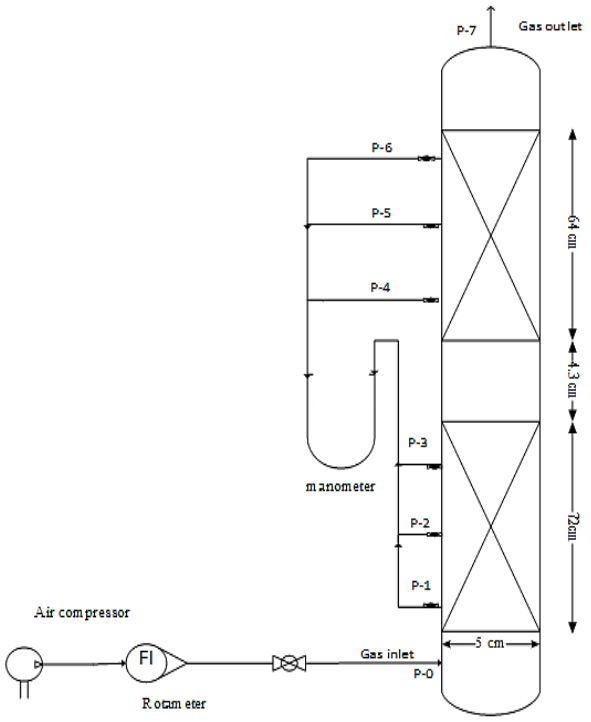

Figure 1. Schematic of experimental set up.

3. Mathematical models

3.1 Fluid dynamic equations

The governing equations describing the gas flow through the packed area are the volume averaged continuity and momentum equations:

Continuity Equation;

$$\frac{\partial}{\partial t}(\varepsilon\gamma\rho) + \nabla.\{\varepsilon(\gamma\rho U - \tau\nabla\gamma)\} = 0 \tag{5}$$

Momentum Equation;

$$\frac{\partial}{\partial t}(\varepsilon\gamma\rho U) + \nabla.\{\varepsilon\gamma(\rho UU - \mu(\nabla U + (\nabla U)^T))\} = \varepsilon\gamma(B - \nabla p) \quad (6)$$

Where:

The porosity of the packing area, ε, the volume fraction occupied by a phase, γ, the fluid density, ρ, the effective viscosity, μ , the dispersion coefficient, τ, the interstitial velocity vector, U, the body force (including the gravity and the flow resistance offered by the packing elements), B, the pressure, p complete continuity and momentum equations

3.2 Body force in packed area

Meandrous spaces in packed areas make resistance to fluid flowing. Body force includes the gravitational force ρg, In addition the resistance increased by the solid packing elements. In this equation (eq.7) $\boldsymbol{R}$ is resistance tensor. Resistance tensor is predictable from pressure drop By Darcy's low (eq.8).

$$B = \rho g + R\,.U \quad (7)$$

$$U = -\,R^{-1}\,.\,\nabla P \quad (8)$$

In this article, pressure drop correlations in Ergun's approach (eq.1) and Reichelt's approach (eq.2) is examined to define gas resistance flowing across the packed areas.

3.3 Porosity distribution

As explained in first section, the influence of confining walls on pressure drop of any packed area is the subject of many studies [11, 17]. Wall effect is defined as radial porosity distribution caused flow tendency near confining walls. Many studies carried out to define radial porosity distribution in packed beds [17], but there isn't any equation described this distribution for all kinds of packing. In this study, de Klerk's approach (eq.13) and packing effective diameter calculations are applied to define radial porosity distribution of packed column of Raschig rings.

$$a = \frac{R - r}{D} \quad (9a)$$

$$\varepsilon(r) = 2.14a^2 - 2.53a + 1 \;, a \le 0.637 \quad (9b)$$

(9c)

$$\varepsilon(r) = \varepsilon_b + 0.29\exp(-0.6a).\left[\cos\left(\frac{2}{3\pi(a - 0.16)}\right)\right] + 0.15\exp(-0.9\,a) \;, a > 0.637$$

4. CFD Simulation

Packed tower described in previous section is applied in simulation. Table 2 shows geometrical properties of packed areas in experimental set-up.

Table 2. Packed area properties.

Effective diameter of the packing element, cm	0.28
Porosity of upper packed area	0.6904
Porosity of lower packed area	0.8303

4.1 Geometry of packed tower

Fig. 2-(a) illustrates three dimensional (3D) geometry of absorption tower with two separated packed areas with exact geometry of gas inlet and outlet. In this simulation packed areas with Raschig rings have been modeled by porous media with fluid flow resistance. Averaged experimental data of porosity has been used in simulation without wall effect consideration.

4.2 Meshing

Figure 2-(b) shows meshed structure of packed absorption tower. Fine and distributed unstructured meshing has been applied specially in characteristic places such as near confining wall, fluid inlet, fluid outlet and distributer holes. The effect of the mesh number was examined on dry pressure drop results in four number of nodes 641908, 707764, 748879, 834808.

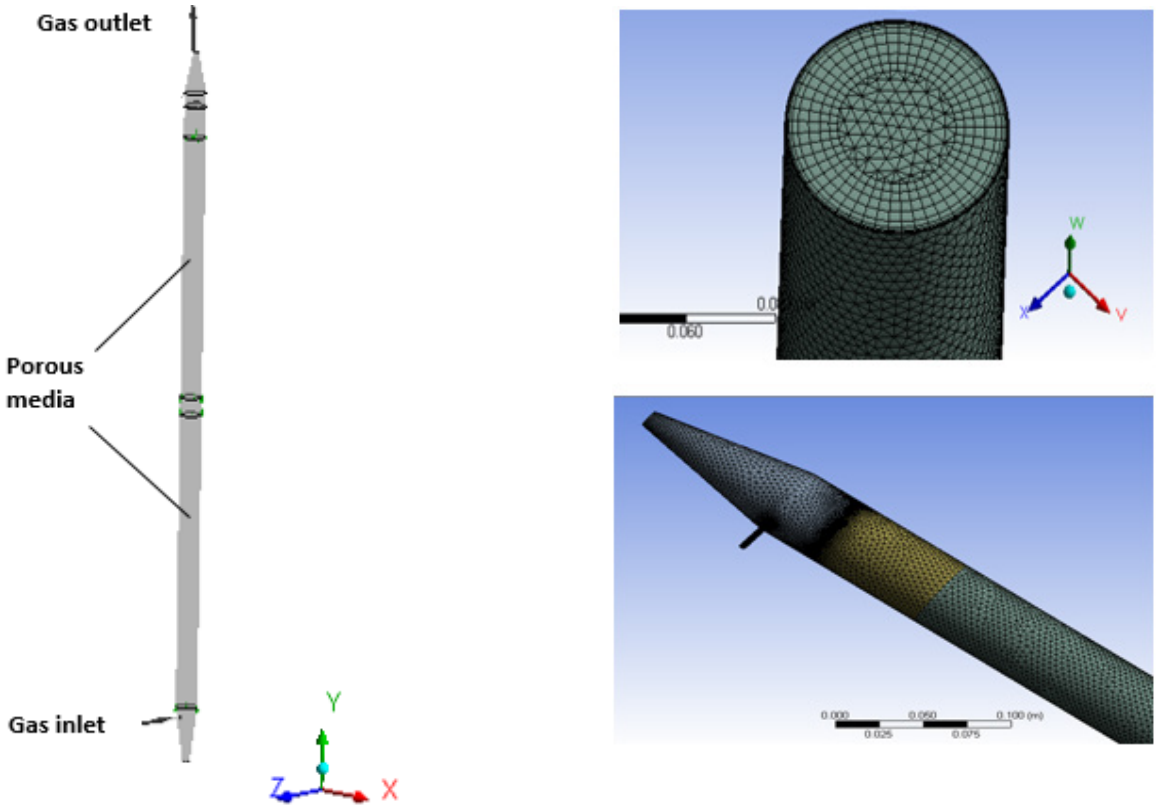

Figure 2. Packed column: (a) geometry and (b) mesh structure

4.3 Fluid flow regime and boundary conditions

Reynolds number calculations shows laminar and transient flow regimes along the tower. Turbulence effect is ignored in the simulation. Fluid velocity is used for inlet condition and constant pressure is used for outlet condition. No-slip condition is used for walls.

5. Result and discussion

5.1 Porosity Effect

In packed reactors it is accepted that radial porosity distribution, $\varepsilon(r)$, is a function of packing diameters but by changing diameter the average porosity remains a constant value at about 0.4. However, the average axial porosity, $\varepsilon(z)$ is varied by repacking in industrial towers with large diameters [20, 25]. Fig.3 illustrates 2D radial porosity distribution has been used by software in x-y coordination.

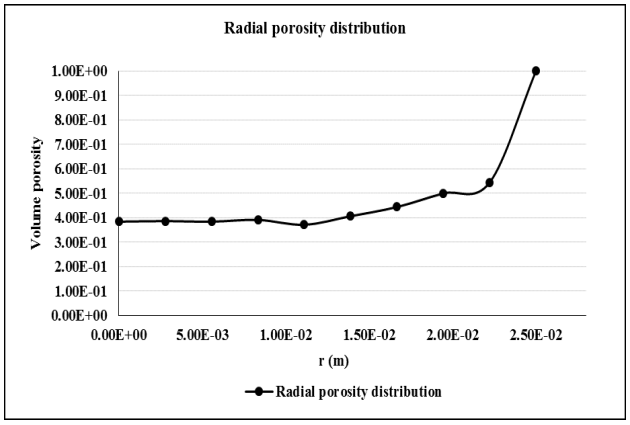

Figure 3. Porosity data generated by CFD model: radial

5.2 Wall Effect and pressure drop

CFD simulation was used to calculate pressure drop in the packed tower. The results compared with experimental data for the model validation in Fig. 4. Fig. 4 demonstrates with increasing gas velocity effects of transient behavior is more profound on the pressure drop. At low gas velocity the experimental data and predicted results are close to each other

but the difference increases at higher gas flow rates; in other word wall effect becomes more characteristic by increase in fluid flow velocity in transient flow regime. Fig.4-(a) shows simulation results using Ergun's, Eq. 1, and de Klerk's, Eq. 13 and 14, equations. Fig.4-(b) shows simulation results using Reichelt's, Eq. 2, and de Klerk's, Eq. 13 and 14, equations. Experimental dry pressure drop is included as well. The figures show that using wall effect relations give a pressure drop estimation with a lesser difference from experimental data. It shows that combination of Ergun-Klerk relation gives more accurate data and therefore is more favorable.

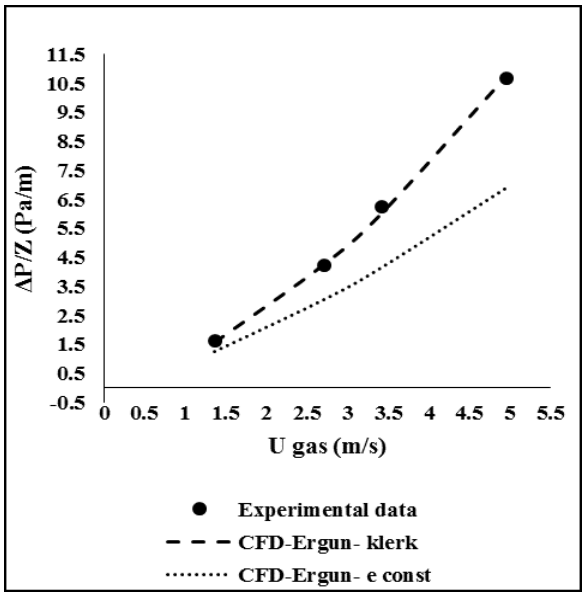

(a)

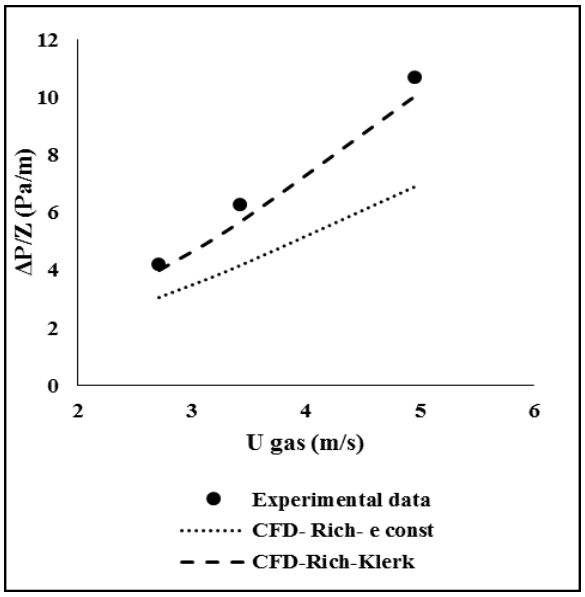

(b)

Figure 4. Wall effect considering by de Klerk's approach study for simulations with pressure drop predicting equations: (a) Ergun (b) Reichelt

In Fig.5 CFD estimated pressure drop data has compared with experimental data. Ergun's approach in pressure drop prediction was more successful than Reichelt's approach in fluid flow resistance description in packed column with column diameter to effective diameter of packing ratio of 17.

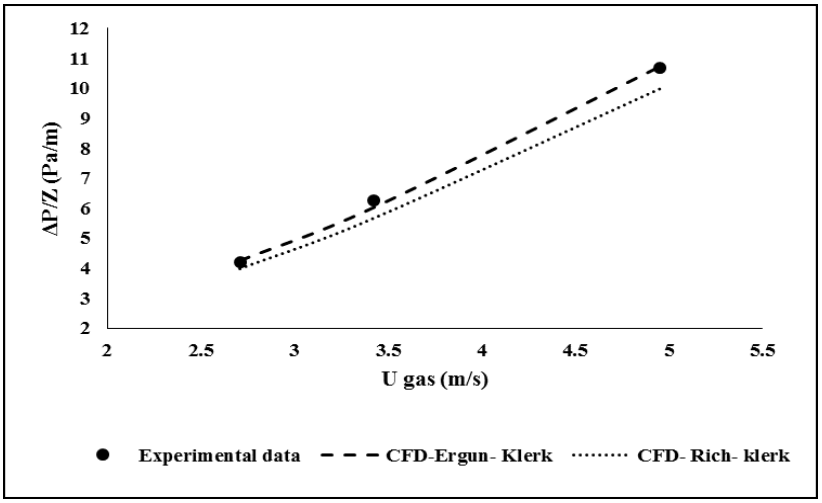

Figure 5. Comparison between Ergun's and Reichelt's approaches in fluid flow resistance description for packed column with Raschig rings

The CFD models errors prediction is illustrated in Fig 6. The de Klerk's approach is about 56% more successful in predicting experimental data regardless of not using wall effect. The de Klerk's description of packed bed geometry has just 4% error (Fig.6 a and b). Using Reichelt's approach to describe fluid flow resistance with wall effect consideration become about 50% more successful in experimental data prediction but has about 10% error yet (Fig.6 c and d). Fig.6 b and d demonstrate simulation by general Ergun's approach in resistance description is 6% more successful than Reichelt's approach in pressure drop prediction.

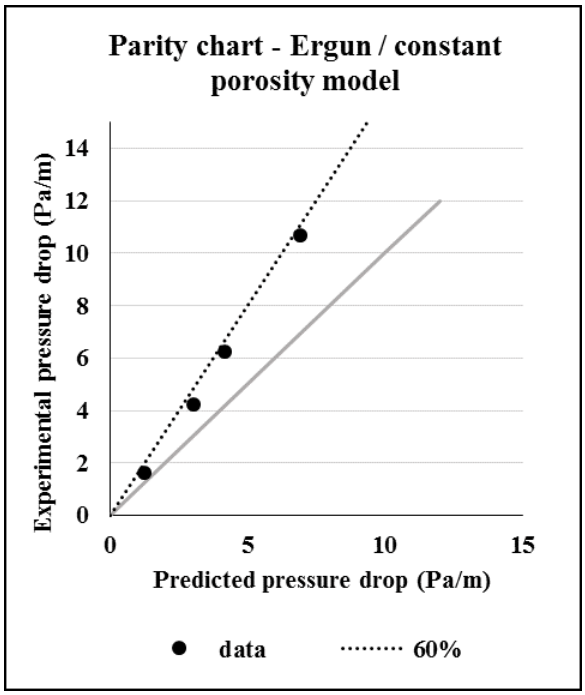

Figure. 6a

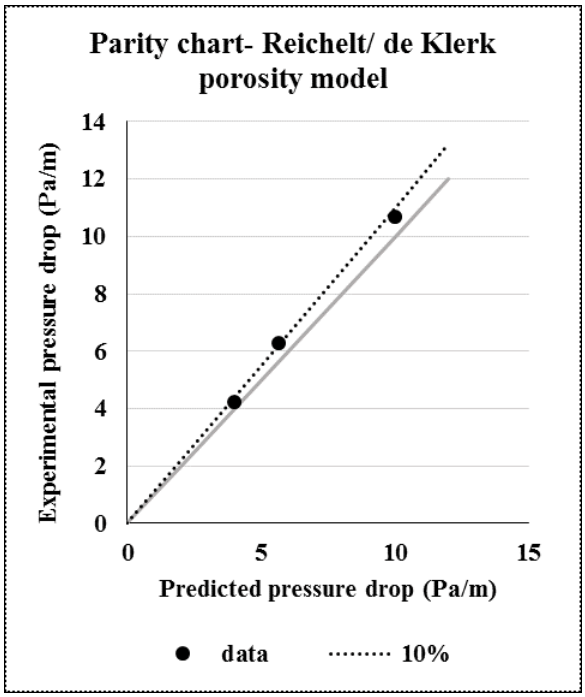

Figure. 6c

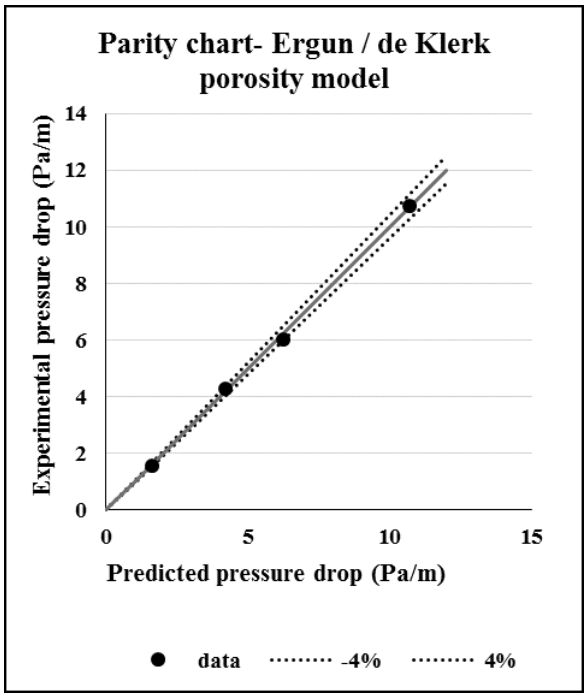

Figure. 6b

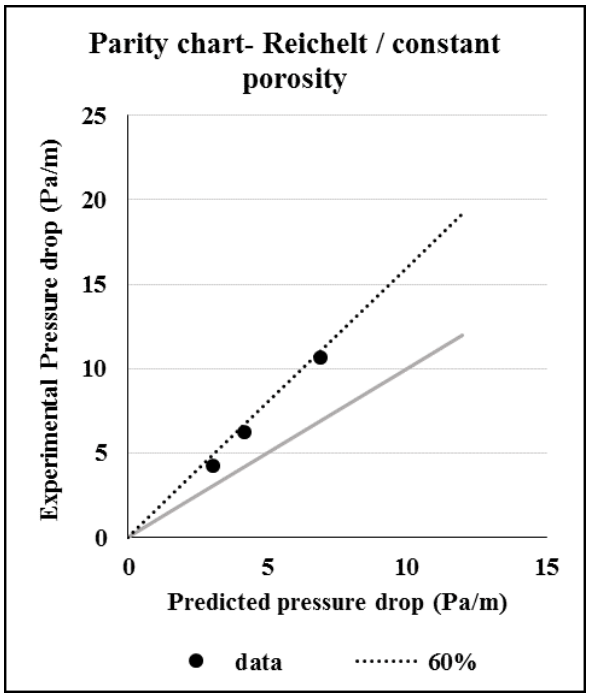

Figure. 6d

Figure 6. The CFD model prediction validation study: (a) and (b) Ergun's approach in resistance description with and without wall effect consideration, respectively. (c) and (d) Reichelt's approach in resistance description with and without wall effect consideration, respectively.

6. Conclusion

In this article packed tower with Raschig rings in pilot scale has been simulated by using porous with resistance model. Wall effect phenomena is examined by de Klerk's approach for effective diameter of packing element. In addition, Ergun's and Reichelt's approaches are examined to describe flow resistance across the packed area. Simulation and modeling validated for dry pressure drop experimentally.

Simulation of packed bed geometry in packed tower with Raschig rings illustrates that wall effect has characteristic role in pressure drop prediction in packed column with column diameter to effective diameter of packing ratio 17. Tomographic experiments is costly and calculation the exact meandrous spaces of packed areas requests advance computation power. de Klerk's approach and effective diameter of a packing calculation was successful in description of Raschig rings packed bed geometry. Although approved Reichelt equation is successful to predict pressure drop in low column diameter to effective diameter of packing ratios, this study demonstrates general Ergun's approach is more successful than Reichelt's approach to describe fluid flow resistance across the packed area in high column diameter to effective diameter of packing ratio 17.

Acknowledgement

The authors wish to acknowledge the support by the University of Sistan and Baluchestan pilot laboratory technicians and staffs.

Nomenclature

A, B	Coefficients of pressure drop equations (-)
a	Nondimensional distance from the wall (-)
a_v	Specific surface of a particle (m^{-1})
$\boldsymbol{B}$	Body force (N)
D	Column diameter (m)
D_p	Equivalent spherical diameter (m)
d_p	Particle diameter (m)
G	Gas flow rate (Kg/ m^2. s)
g	Acceleration due to gravity (m/s^2)
Δp	Pressure drop across packed bed (Pa)
R	Resistance tensor kg $s^{-1}m^{-3}$
R	Column radius (m)
r	Radial position relative to the column center line (m)
Sp	Surface area of particle (m^2)
U	Superficial gas velocity (m/s)
us	Superficial fluid velocity (m/s)
Vp	Volume of particle (m^3)
Z	Height of packed bed (m)

Greek letters

μ	Dynamic viscosity (N s/m^2)
ε	Porosity (-)
εb	Porosity in the absence of wall effects (-)
y	Volume fraction(-)
ρ	Density (kg/m^3)
ρg	Gas density (kg/m^3)
$\emptyset_S$	Sphericity coefficient (-)
ε	Dispersion coefficient vector, $kgm^{-1}s^{-1}$

References

1. Y. Haroun., L. Raynal," Use of Computational Fluid Dynamics for Absorption Packed Column Design", Oil and Gas Science and Technology - Rev. IFP Energies nouvelles, 71, 43,(2016).

2. Liu, Q.S., Roux, B., Velarde, M.G., "Thermocapillary Convection in Two-Layer Systems", International Journal of Heat and Mass Transfer, 41(11), 1499(1998).

3. Ludwig, Applied Process Design for Chemical and Petrochemical Plants, 3rd ed., 2, Gulf Professional Publishing, 230(1979).

4. Leva, M., Weintraub, M., Grummer, M., Pollchik, M., & Storch, H. H. Fluid Flow through packed and Fluidized systems. United States, Bureau of Mines, Bulletin 504 (1951).

5. E. Ozahi, Gundogdu, M.Y., Carpinlioglu, M.O., "A Modification on Ergun's Correlation for Use in Cylindrical Packed Beds With Non-spherical Particles",Advanced Powder Technology,19,369(2008).

6. Wu, J., Yu, B., Yun, M., "A resistance model for flow through porous media" Transp Porous Med,71, 331(2008).

7. [7] S. Ergun, Fluid flow through packed columns, Chem. Eng. Prog. 48, 89(1952).

8. Cohen, Y., Metzener, A. B.,"Wall Effects in Laminar Flow of Fluids through Pocked Beds", AlChEJ, 27(5), 705 (1981).

9. Foumeny, E. A., Benyahia, F., Castro, J. A. A., Moallemi, H. A., Roshani, S., "Correlations of pressure drop in packed beds taking into account the effect of confining wall", International Journal of Heat and Mass Transfer, 36(2), 536 (1993).

10. W. Reichelt, Zur Berechnung des Druckverlustes einphasig durchströmter Kugel- und Zylinderschüttungen, Chem. Ing. Tech., 44, 1068 (1972).

11. Eisfeld. B., Schnitzlein. K., "The influence of confining walls on the pressure drop in packed beds", Chem. Eng. Sci., 56, 4321 (2001).

12. Atmakidis, T., Y. Kenig, E., "CFD-based analysis of the wall effect on the pressure drop in packed beds with moderate tube/particle diameter ratios in the laminar flow regime", Chem. Eng. J., 155, 404(2009).

13. D. Sebastia-Saez et al."Meso-scale CFD study of the pressure drop, liquid hold-up, interfacialarea and mass transfer in structured packing materials", International Journal of Greenhouse Gas Control, 42, 399 (2015).

14. Caulkin,R., Jia, X., Fairweather, M., Williams, R.A., "Predictions of Porosity and Fluid Distribution through Nonspherical-Packed Columns", AIChEJ, 58(5), 1503 (2012).

15. Boyer, C., Koudil, A., "Study of liquid spreading from a point source in a trickle bed via gamma-ray tomogeraphy and CFD simulation", Chem. Eng. Sci., 60, 6279(2005).

16. Liu, S., Long, J.," Gas-liquid countercurrent through packed towers", Journal of Porous Media, 2(2), 99(2000).

17. de Klerk, A.," Voidage Variation in Packed Beds at Small Column to Particle Diameter Ratio", AIChEJ, 49(8), 2022(2003).

18. Sun C. G., Yin. F. H., Afcan. A., Nandakumar. K., and Chuang. K. T., "Modeling and Simulation of Flow maldistribution in random packed columns with gas-liquid countercurrent flow", Trans. IChemE, 78(Part A), 378 (2000).

19. Yin F. H., Sun C. G., Afacan A., Nandakumar K., Chuang K. T.," CFD Modeling of Mass-Transfer Processes in Randomly Packed Distillation Columns," Ind. Eng. Chem. Res., 39, 1369(2000).

20. Jiang Y., Khadilkar Mohan R., Al-Dahhan Muthanna H., Dudukovi Milorad P.," CFD modeling of multiphase flow distribution in

catalytic packed bed reactors: scale down issue", Catalysis Today, 66, 209(2001).

21. Liu G.B., Yu K.T., Yuan, X.G., Liu C.J., Guo Q.C., "Simulations of chemical absorption in pilot-scale and industrial-scale packed columns by computational mass transfer", Chem. Eng. Sci., 61, 6511(2006).

22. Liu,G,B .,Yu ,K.T., "A numerical method for predicting the performance of a randomly packed distillation column" , International Journal of Heat and Mass Transfer, 52 ,5330(2009).

23. Fourati, M., Roig, V., Raynal, L.,"Liquid dispersion in packed columns: Experiments and Numerical modeling", Chem. Eng. Sci. (2013).

24. Geankoplis, Christie J. Transport Process and Unit Operations.3rd ed. Prentice Hall: New Jersey , chapter 3 (2003).

25. Iliuta I., Larachi F., "Three-dimensional simulation of gas-liquid concurrent down flow in vertical, inclined, and oscillating packed beds, AIChEJ, 62(3), p.916(2016).

Effect of Coating Method and Feed Pressure and Temperature on CO_2/CH_4 Gas Separation Performance of Pebax/PES Composite Membranes

• **Hamid Reza Afshoun[1], Mahdi Pourafshari Chenar[1*], and Ahmad Fauzi Ismail[2]**
1. Chemical Engineering Department, Faculty of Engineering, Ferdowsi University of Mashhad, Mashhad, Iran
2. Advanced Membrane Technology Research Centre (AMTEC), University Technology Malaysia, Malaysi
Corresponding author Email address: pourafshari@um.ac.ir

Received: Mar. 31, 2017 / Accepted: Apr. 20, 2017

Abstract

In this study, PES/Pebax composite membranes were prepared by coating the porous PES support layers by Pebax-1657. Film casting and pouring methods were used for coating Pebax layer. The effects of coating technique and conditions including coating solution concentration and curing temperature on CO_2 and CH_4 gas permeabilities of prepared composite membranes were investigated. SEM images were used to investigate the structure of the prepared membranes. Pure CH_4 and CO_2 gases were used to investigate the gas permeation properties of the prepared membranes at different trans-membrane pressures (1-11 bar) and feed temperatures (25-55°C). The obtained data showed that the prepared PES supports did not provide any CO_2/CH_4 selectivity. The results also showed the CO_2/CH_4 selectivity for the membrane prepared via pouring technique was higher than that of the film casting procedure due to the defect-free Pebax layer formation. CO_2 and CH_4 permeance increased as the feed temperature increased from 25 to 55°C. The results also showed that CO_2 permeance increased from 6.8 to 10.1 GPU with an increase in feed pressure from 2 to 12 barg, while CH_4 permeance remained almost constant and CO_2/CH_4 selectivity increased from 27 to 42.

Keywords: Pebax, Composite membrane, CO_2 separation, Coating method, Feed pressure, temperature.

1. INTRODUCTION

Membrane gas separation has been interested by many researchers due to the advantages of the membrane systems. Natural gas sweetening, including separation of carbon dioxide and hydrogen sulfide from the natural gas, is an example of membrane application in gas separation (Yampolskii and Freeman, 2010).

Inorganic membranes containing ceramic or metal membranes and organic membranes such as cellulose acetate, polysulfone (PSf), polyethersulfone (PES) and polyetherimide (PEI) have been investigated for gas separation applications (Ismail et al., 2015). Organic materials have been used and studied more than inorganic materials due to their low cost and simplicity in the membrane preparation.

Polymers used in the membrane preparation are divided into two groups of glassy and rubbery polymers. Glassy polymers are those polymers that their glass transition temperature is higher than the operating temperature; and in rubbery polymers, the glass transition temperature is lower than the operating temperature (Baker, 2004). The behavior of these two polymers in gas separation is different and for rubbery polymers the difference between gases' solubility in polymer is the key parameter of separation. The solubility of condensable gases such as carbon dioxide is often more than that of gases with low condensability, such as methane (Matsuura, 1993).

Selectivity and permeability are two important parameters in the membrane gas separation, and when they are high, it shows the high performance of the membrane. There is a limit to the polymeric membrane performance and it is the reveres behavior of selectivity and permeability. High permeability of the membranes leads to the low selectivity and vice versa. Robeson has examined this behavior and provided some diagrams for the used polymers and different gas separations which are known as the Robeson's upper bounds (Robeson, 2008) and new synthetic membranes are often compared with these plots.

Studies on the use of membranes for gas separation applications usually include, synthesis of new polymers with higher selectivity and permeability (Wijenayake et al., 2014), addition of inorganic or organic additives into the membranes (mixed matrix membranes) to increase their performance [7-16], examining the effect of operating and preparation conditions on the membrane separation performance (Choi et al., 2010) and preparation of multi-layer composite membranes to improve the membrane performance (Ren et al., 2012, Li et al., 2013b, Ramon et al., 2012, Yong et al., 2013)

Composite membranes that have been used in many studies include coating of at least one polymer layer on the surface of another polymer. The upper layer is usually a rubbery polymer that is coated on the substrate (sublayer) which is a glassy polymer (Vankelecom et al., 1999). The upper layer is used for the two following purposes:

- Enhancing the selectivity with coating the pores and surface defects in the bottom layer
- Using the upper layer as a selective layer for gas separations.
-

In the second case, the upper layer acts as a selective layer. The bottom layer which is a glassy polymer acts as an anchoring and guarantees the mechanical strength of the membrane. The upper layer which is a very thin layer also leads to the membrane selectivity. If the thickness of the upper layer decreases, then the permeance of the resulting membrane will increase. However, if the thickness of the selective layer decreases much, the probability of the defectless coating will decrease and in the case of defect in the upper layer, the selectivity will decrease. Some studies have been done on the effects of effective factors on the performance of the composite membranes such as preparation conditions (coating method) (Madaeni et al., 2013, Kargari et al., 2014, Choi et al., 2015), sublayer characteristics (Ramon et al., 2012, Zhu et al., 2015), upper layer thickness and using the middle layer (Li et al., 2013a).

There are several methods to prepare composite membranes (Ismail et al., 2015, Baker,

2004) such as casting, dip-coating and interfacial polymerization. For example, for hollow fiber membrane preparation, using the dip-coating method is more effective. Extrusion and press method are also used for making composite membranes (Bennett et al., 1997). Madaeni et al. (Madaeni et al., 2013) studied the effect of coating method (film casting and dip-coating methods) on gas separation performance of PDMS/PES composite membranes. In the film casting method, top layer materials are coated on the surface of substrate by film applicators or home-made blades. In dip-coating, the top layer is formed by immersing substrate in an appropriate polymer solution. They concluded that for similar concentration of coating solution in single coating, selectivity for the membrane prepared via film casting technique was higher compared to that of the dip-coating procedure due to the thicker coated layer in film casting method. However, its permeability was lower.

In recent years, a huge number of studies focused on development of PEO-based membranes for gas separation. These studies have eventuated in different grades of Pebax such as 1074, 1657, 2533, and 3533 (Li et al., 2013b, Reijerkerk et al., 2011, Car et al., 2008a, Car et al., 2008b, Murali et al., 2014, Murali et al., 2010, Liu et al., 2004, Nafisi and Hägg, 2014, Scofield et al., 2016, Mosleh et al., 2015). These copolymers have been used as pure or mixed with other ingredients for membrane gas separation applications (Cheng et al., 2015, Cheng et al., 2016, Lillepärg et al., 2016).

Pebax as a rubbery polymer has been used for CO_2/CH_4 separation in recent studies (Ren et al., 2012, Scofield et al., 2016). Pebax is a copolymer that is formed from the soft segments of polyethylene oxide and the hard segments of polyamide and according to the type and ratio of these two parts, there are commercially various types of them that have been investigated by researchers in gas separation applications (Li et al., 2013b, Reijerkerk et al., 2011, Murali et al., 2010, Car et al., 2008a, Murali et al., 2014, Nafisi and Hägg, 2014). This copolymer tends to absorb carbon dioxide, because it contains carboxyl groups and it is used to separate this gas from light gases such as methane. Usually, it is used as a coating layer on a porous surface called a composite membrane. In this case, a thin layer of Pebax performs the separation as a selective layer.

In this study, PES was selected as support and commercial Poly (amide-6-b-ethylene oxide) (Pebax MH 1657) copolymer, composed of 60 wt% of PEO and 40 wt% of PA6 (nylon-6), was selected as selective layer to prepare flat sheet Pebax/PES composite membranes. The main purpose of this study was investigating the effect of coating method on performance of Pebax/PES composite membrane for CO_2/CH_4 gas separation. Film casting and pouring methods were used to coat the Pebax layer on PES supports. The effect of feed pressure and temperature on gas separation properties of prepared membrane was also investigated.

2. Experimental

A. Materials

Pebax-1657 which is a copolymer and is composed of polyamide and polyethylene oxide and PES were provided by Arkema Inc., France. Ethanol (EtOH) and dimethyleformamid (DMF) were purchased from Merck Co., Germany, and used as solvents in this study. The gas permeation experiments were conducted using pure CH_4 and CO_2 gases with purity of 99.99%.

B. Preparation of Pebax dense membrane

Pebax-1657 copolymer was dried in an oven at 60˚C for 48 h to remove moisture content in the polymer. 4wt% Pebax-1657 solution was prepared by gradually adding Pebax pellets into the solvent mixture of ethanol/water (70/30 vol/vol). For the complete dissolution of polymer pellets, the solution was vigorously stirred and kept under reflux at 75˚C for 4 h. Since the polymer does not dissolve in the ethanol/water mixture at low temperatures, the temperature control plays a key role in the solution preparation. After complete dissolution of polymer, the solution was gradually cooled

to the room temperature.

Solution casting and solvent evaporation techniques were used to prepare the dense films. Bubble free Pebax solution was cast on the uniform and clear glass plate and the solvent was evaporated to obtain a dense film. For complete removing the trace amount of solvent in the membrane, the obtained dense film was further dried at ambient temperature for 24 h and subsequently dried in the oven at 40˚C for 24 h.

C. Preparation of composite membranes

Composite membranes were prepared by coating the selective thin layer of Pebax on the surface of PES porous supports. PES porous support membranes were also prepared by phase inversion technique. 18wt% PES solution was prepared by dissolving the polymer in DMF solvent under constant mechanical stirring speed of 200 rpm at ambient temperature. The completely dissolved polymer solution was sonicated for 6 h to remove the air bubbles. The homogeneous and bubble free solution was cast on the glass plate with the indigenously designed casting knife. The prepared films were immersed in distilled water bath for precipitation. Subsequently, membranes were immersed in fresh distilled water for 24 h for complete removal of solvent. The prepared membranes were dried for 24 h at ambient temperature. Dried and porous PES support layers were tested with pure gases.

The composite membranes were prepared by coating Pebax solution on the PES porous sublayers. Casting method and pouring were used in this study to coat the Pebax layer. In casting method, considering the porous nature of the substrate and the low thickness of the selective layer, it is difficult to obtain defect-free coated surface. In pouring method, PES membranes were attached to the glass plate and kept at an angle of 45°C . Using a dropper, specific amount of bubble-free Pebax solution was dropped on the PES surface. Membranes were dried at room temperature for 24 h. After that, membranes were kept in the oven at 40˚C for 24 h.

D. Pure gases permeability

Gas permeation tests were performed using a constant pressure - variable volume system described elsewhere (Ismail and Lai, 2003). The membrane to be tested is placed into the membrane test cell with an effective permeation area of 13.5cm^2. The feed gas, CO_2 or CH_4, was passed on the upstream side of the membrane and the desired pressure was maintained. The downstream side pressure was ambient pressure. By measuring the volume changes with the time (Q), the gas permeability is calculated from the Eq. 1.

$$P = \left(\frac{Q.L}{A(p_1 - p_2)}\right)\left(\frac{273.15}{T}\right)\left(\frac{p_2}{76}\right) \quad (1)$$

Ideal selectivity (permselectivity) of membranes is calculated as the ratio of gas permeabilities:

$$\alpha_{CO_2/CH_4} = \frac{P_{CO_2}}{P_{CH_4}} \quad (2)$$

where P is the permeability coefficient, barrer (1 barrer = 10^{-10} cm^3(STP).cm/cm^2.s.cmHg), Q is the permeation flow rate (cm3/s), L is thickness of the membrane (cm), A is the effective membrane area (cm^2), p_1 and p_2 are the absolute pressure (cmHg) of two sides of the membrane, and T (K) is the absolute temperature of tested gas. If the thickness of the active layer of membrane is not measured accurately, the permeance (P/L) of the gases is calculated. The gas permeance unit is GPU (1GPU=10^{-6} cm^3(STP)/cm^2.s.cmHg).

Membranes were tested four times with each gas to determine the repeatability and consistency of results. In composite membranes, coating solution penetrates into the pores of the substrate, hence, it is not possible to determine the exact thickness of the effective selective layer. Therefore the permeance data was reported instead of the permeability in tables and charts.

E. Scanning electron microscopy (SEM)

The SEM images were used to see the structure of prepared membranes. Scanning electron microscopy (SEM) images were also used to measure the thickness of the Pebax layer in composite membranes. SEM images of PES supports and composite membranes were taken with a HITACHI Model TM3000 SEM machine. Membranes were fractured in liquid nitrogen to obtain clean cut for cross sectional view. The samples were then gold sputtered for producing electrical conductivity.

3. Results and discussion

A. SEM images of synthesized membranes

Figs. 1 and 2 present the SEM images of support layer without coating and composite membranes that were synthesized and used in this study. Surface images were shown in Fig. 1. Fig. 1a presents the PES support that was porous and the surface pores can be seen in the images. Different solvents used for the polymer solution behave differently during phase inversion, which might also affect the porous structure of membrane. Fig. 1b presents the composite membrane surface. As can be seen, after coating, there is no pores on composite membrane surface and the surface is smooth.

SEM images of composite membrane surface demonstrated that the dense Pebax layer was coated uniformly on the surface of porous support membranes.

Fig. 2 presents the cross sectional images of composite and Pebax dense membranes. Based on the cross sectional images, no splits were found at the interface between the Pebax layer and the supports. Composite membranes were synthesized by varying the active layer thickness by coating with different thicknesses of Pebax solution on the sublayers. Figs. 2a, 2b and 2c present cross sectional SEM images that were made with two coating methods. The active layer thicknesses were different. Fig. 2a presents the cross sectional image of membrane that was prepared by pouring method and Figs. 2b and 2c present the cross sectional images of membranes that were prepared by film casting method. The top layer thicknesses in Figs. 2b and 2c were different.and 2c were different.

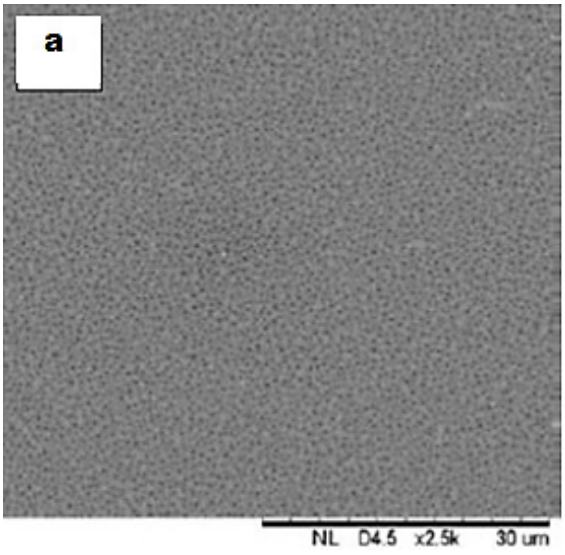

NL D4.5 ×2.5k 30µm

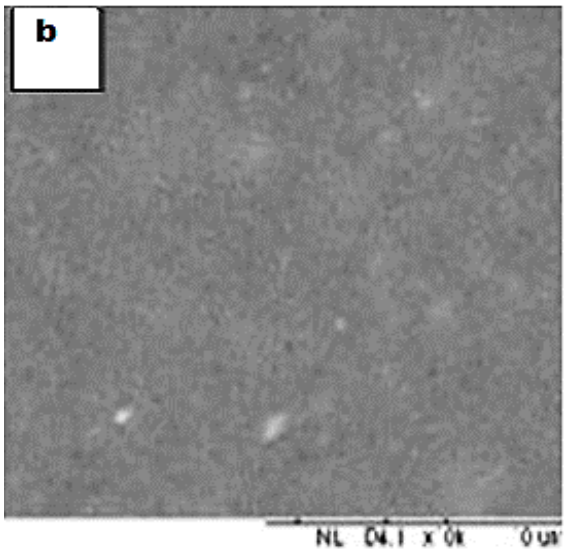

NL D4.5 ×2.5k 30µm

Figure 1. SEM images of (a) PES support surface and (b) composite membrane surface

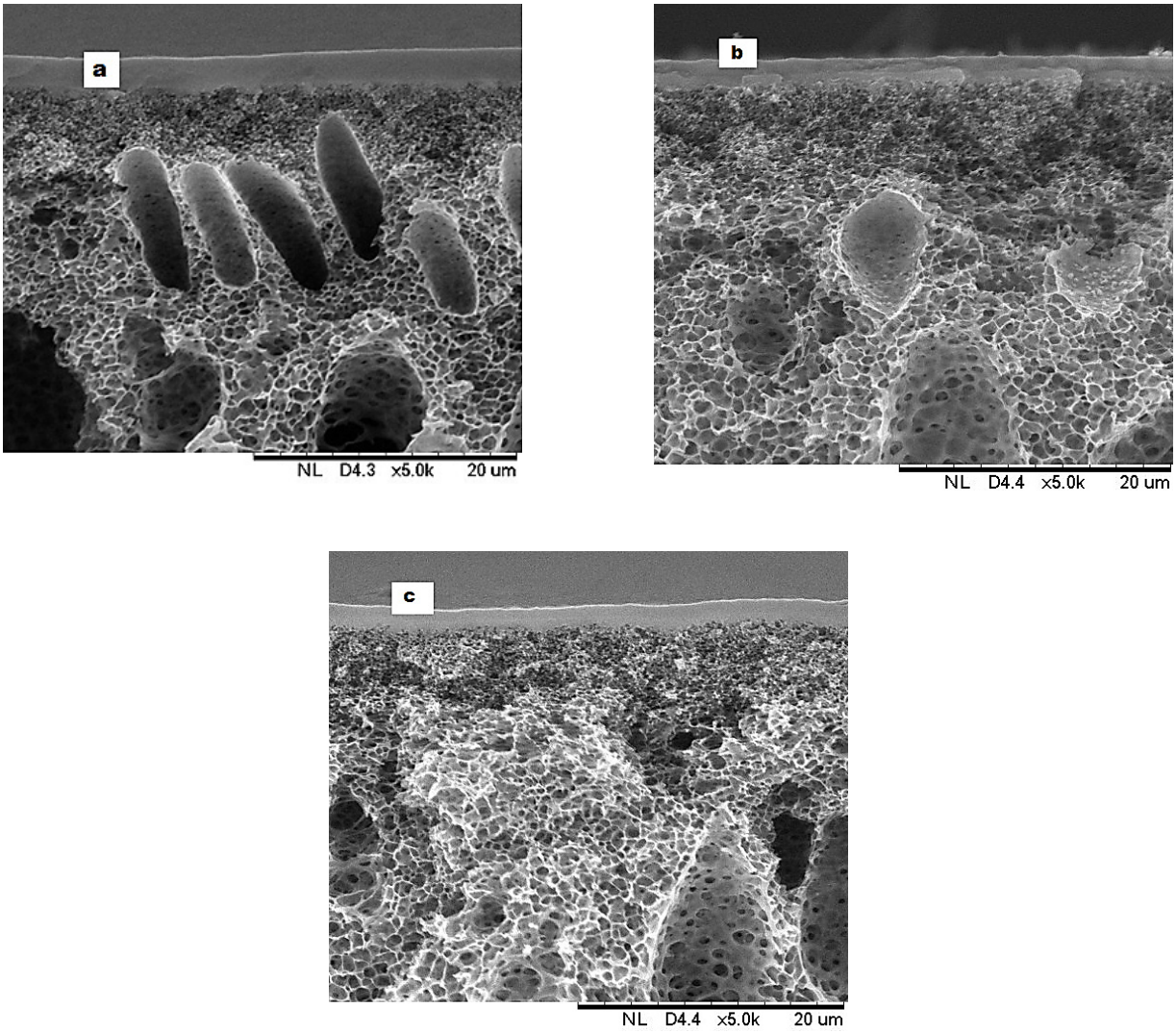

Figure 2. SEM cross sectional images of PES/Pebax composite membranes; (a) prepared by pouring method, (b, c) prepared by film casting method with different Pebax thicknesses

B. Pure gas permeation test

Pure CH_4 and CO_2 gases were used to determine the performance of the synthesized membranes. Initially, gas permeation properties were determined for the porous PES membrane that was synthesized by phase inversion method. Permeances of both CH_4 and CO_2 gases for PES membrane at feed pressure and temperature of 1 barg (gauge pressure) and 25°C were shown in Table 1, which reveals that the support layer has less resistance for the gas permeation.

Table 1. CO_2 and CH_4 pure gas test results of supports and dense Pebax membranes

Membrane sample	CO_2 permeance (GPU)	CO_2/CH_4 selectivity
PES support	3700 ± 50	1.0
Dense Pebax	1.3 ± 0.05	26

The Pebax dense membrane that was prepared with thickness of 50μm was also tested to measure the Pebax permeability at feed pressure and temperature of 4 barg and 25 ˚C and the obtained data was presented in Table 1. By considering the thickness of Pebax membrane (50 μm) that was determined by a digital micrometer, the permeability of carbon dioxide was 65 barrer. The CO_2 permeability for Pebax 1657 was reported as 55.8 and 72 barrer in other studies (Murali et al., 2014, Li et al., 2013b). As shown in Table 1, for support layer without coating, there was no selectivity because of its high porosity.

The properties of CO_2 and CH_4 gases have been listed in Table 2. It could be understood that the permeability of gases in rubbery membranes was mainly controlled by sorption and solubility. As mentioned previously, Pebax is a rubbery polymer and according to Table 2, due to the higher critical temperature of CO_2 than CH4, that means the higher condensability of CO_2, the permeance of CO_2 should be much higher than CH_4 as it has been proved from Table 1. For Pebax dense membrane the CO_2/CH_4 selectivity was 26 as shown in Table 1.

C. Effect of top layer coating method

One of the most important factors that affect permeation properties of composite membranes is coating technique. Film casting and pouring methods that are commonly used in composite membranes preparation, were compared in this study and the best method that has shown better separation properties has been introduced. Membranes were prepared by two methods of film casting and pouring and were tested by methane and carbon dioxide pure gases. In both methods, 4wt% Pebax solution in ethanol/water (70/30 vol/vol) is used for coating. In casting method the membranes was prepared by two different top layer thicknesses. For this purpose, different Pebax film thicknesses are considered for casting. After drying, the thickness of the upper layer has been identified by composite membranes cross sectional SEM images. The obtained results are presented in Table 3.

Table 2. Physical properties of CO_2 and CH_4 gases

Gas	Critical volume (cm^3/mol)	Kinetic diameter (Å)	Critical temperature (K)
CO_2	94.07	3.30	304.12
CH_4	98.6	3.82	190.56

Table 3. Pure CO_2 and CH_4 permeances of Pebax/PES composite membranes at feed pressure and temperature of 4 barg and 25 °C

Membrane sample	Top layer coating method	Pebax layer thickness (μm)	CO_2 permeance (GPU)	CH_4 permeance (GPU)	CO_2/CH_4 Selectivity
①	Pouring	2.6	8	0.28	**28**
②	Solution casting	1.7	8.6	0.53	**18**
③	Solution casting	2.4	7.2	0.42	**19.5**

As can be seen in Table 3, the prepared membranes by pouring method, as previously described, had higher CO_2/CH_4 selectivity and it is closer to the selectivity of dense Pebax membranes that was reported in Table 1. The high selectivity indicates better and defect-free coating. For samples No. 2 and 3 which were made by film casting method, from Table 3, the results show that the selectivity obtained for these samples is below the selectivity of dense Pebax membrane. The low selectivity in these samples is because of the defects were created during top layer formation. The existence of the pores causes methane and carbon dioxide to pass through these pores with the same rate. Therefore the membrane selectivity decreased. In sample No. 3, where the thickness of Pebax layer is higher, selectivity improved and permeability reduced. Increasing the thickness of upper layer leads to decrease in the probability of formation of large pores on the surface and the selectivity improves. By increasing the thickness of Pebax layer, the resistance of prepared membrane increased and in result the permeability decreased. In samples No. 1 and sample 3, the thickness of the selective layer is almost the same but CO_2/CH_4 selectivity in sample No. 1 is much more than that of sample No. 3 and this indicates that the coating method is important in identifying the gas separation properties of membranes. To achieve higher selectivity in coated membranes through film casting method, the thickness of upper layer should be increased and in turn the permeability will decrease. The difference in the permeability of membranes prepared with two methods depends on the overall resistance of composite membranes for gases.

D. Effect of feed pressure

The effect of feed pressure on permeability of gases in polymeric membranes depends on the polymer and gas structures. In rubbery membranes, the permeability of light gases is independent of pressure and by increasing the pressure, the permeability remains constant but the permeability of gases with high condensability the permeability increases by feed pressure increment (Freeman et al., 2006). This increase in permeability is because of increasing gas absorption and solubility in membrane. Considering the fact that permeability of light gases (methane, hydrogen, ...) does not change with increasing the pressure, so the selectivity of rubbery membrane increases with increasing the pressure. Therefore, by increasing the feed pressure of the CO_2 pure gas, its permeability increases but for methane, the permeability is independent of pressure and because of this the CO_2/CH_4 selectivity increases by increasing the pressure. Figure 3 shows the CO_2 permeability and CO_2/CH_4 selectivity data and feed pressure for prepared composite membranes. Feed temperature is constant and was 25°C and feed pressure has been increased from 2 to 12 barg.

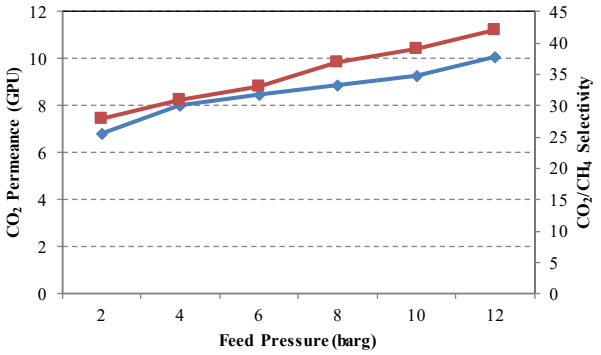

Figure 3. CO_2 permeance and CO_2/CH_4 selectivity versus feed pressure

In Fig. 3, it is observed that by increasing the feed pressure at constant temperature for pure gases, the carbon dioxide permeability and the CO_2/CH_4 selectivity have increased and as it was mentioned before, this behavior has been previously seen in rubbery membranes (Freeman et al., 2006).

E. Effect of feed temperature

Temperature plays an essential role in the separation properties of the membranes. Usually, the permeability of the components increases by increasing the temperature. The influence of temperature on permeability of pure gases of methane and carbon dioxide for Pebax/PES membrane has been investigated. The CO_2 and CH_4 permeability has been measured at three

temperatures of 25, 40, 55 °C and feed pressures of 2 and 4 barg. The obtained results are shown in Table 4. In this table, the relative selectivity that equals the selectivity of CO_2 /CH_2 at any temperature divided to selectivity at 298 K to show the selectivity reduction.

The temperature-dependence of the permeability is typically described by Arrhenius-like equations (Freeman et al., 2006):

$$P_A = P_{A0} \times \exp\left(-\frac{E_P}{RT}\right) \quad (3)$$

In the above equation, P_A is the permeability at temperature T, P_{A0} is the constant coefficient which is constant for each component and E_P is the activation energy of permeability. E_P with the equation (4) is related to E_D, activation energy of diffusion and enthalpy of sorption, ΔH_S.

$$E_P = E_D + \Delta H_S \quad (4)$$

The enthalpy of sorption can be thought of in terms of two contributions: where ΔH_{cond} is the enthalpy of condensation of the pure gaseous penetrant to the liquid phase and ΔH_{mix} is the partial molar enthalpy of mixing the condensed (or compressed) penetrant with the polymer segments. Therefore equation (4) can be written as follow:

$$E_P = E_D + \Delta H_{cond} + \Delta H_{mix} \quad (5)$$

The activation energy of diffusion is usually positive and it increases by increasing the size of the penetrating component. Condensation is energy producer and enthalpy change resulting from condensation of components is negative. By increasing the condensability of components, the absolute value of the enthalpy of condensation will also increase. Enthalpy of mixing can be positive or negative, and it depends on the interactions between components and polymer. If there is a strong interaction between the component and the polymer chain, the enthalpy of mixing will be negative. Since the size of the methane molecule is larger than carbon dioxide, methane E_D is greater. Due to the high tendency of carbon dioxide to turn liquid and the strong interaction between the two polar bonds of CO_2 and ether groups in Pebax, the enthalpy of mixing and condensation of carbon dioxide is negative. Therefore, the E_P of methane is greater and at a similar temperature change, the permeability of methane increases more than carbon dioxide and in result the CO_2/CH_4 selectivity decreases by increasing the temperature. In Table 4, this reduction in selectivity by increasing temperature is observed. To better show the methane and carbon dioxide permeation change by temperature, the results were described in Figures 4 and 5. As can be seen, for both gases, permeance increased with increasing temperature. For both gases at 4 barg the permeance increased more than of increasing permeance at 2 barg for the same increasing in temperature. This behavior can be due to the fact that at higher pressures, the amount of existing gas in polymer is more and increasing the temperature leads to the more increase in both gasses diffusion, and the permeance increased more. But the CO_2/CH_4 selectivity reduction as reported in Table 4 is the same at both pressures.

Table 4. Pure CO_2 and CH_4 permeability for Pebax/PES composite membranes at different feed pressures and temperatures

Pressure (barg)	Temperature (K)	CO_2 permeance (GPU)	CH_4 permeance (GPU)	Relative selectivity
2	298	0.93	0.078	**1**
2	313	1.1	0.113	**0.81**
2	328	1.27	0.144	**0.74**
4	298	1.23	0.094	**1**
4	313	1.92	0.179	**0.82**
4	328	2.40	0.242	**0.75**

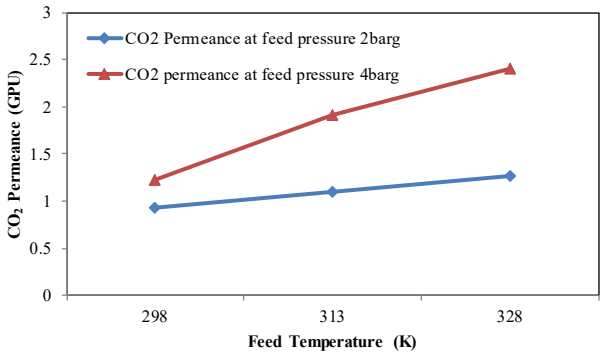

Figure 4. CO_2 permeance at different feed pressures versus feed temperature for Pebax/PES membrane

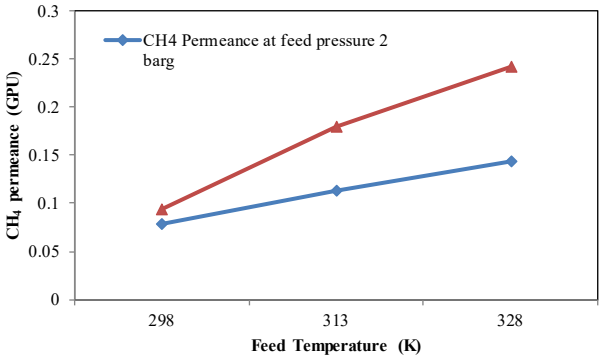

Figure 5. CH_4 permeance at different feed pressures versus feed temperature of Pebax/PES membrane

4. Conclusions

In this study, the effect of coating procedure (film casting and pouring) on the performance of prepared Pebax/PES composite membranes for separation of CO_2/CH_4 was investigated. The results showed that the CO_2/CH_4 selectivity for the membrane that was prepared via pouring technique was higher compared to the film casting procedure due to the defect-free Pebax layer formation. For film casting method, the CO_2/CH_4 selectivity was enhanced from 18 to 19.5 by increasing the top layer thickness from 1.7 to 2.4µm. CO_2 and CH_4 permeance increased as the feed temperature increased from 25 to 55°C. The effect of temperature on CH_4 permeance was dominated and in result the CO_2/CH_4 selectivity of Pebax/PES membranes decreased. The effect of feed pressure on performance of prepared Pebax/PES membranes was also studied. The results showed that CO_2 permeance increased from 6.8 to 10.1GPU with an increase in feed pressure from 2 to 12barg, while CH_4 permeance was remained constant and the CO_2/CH_4 selectivity increased from 27 to 42.

Acknowledgment

Authors would like to gratefully acknowledge Khorasan Razavi Gas Co. of Iran for their financial support.

References

1. Baker, R. W. 2004. Membrane technology and applications. John Wiley & Sons Ltd.

2. Bennett, M., Brisdon, B., England, R. & Field, R. 1997. Performance of PDMS and organofunctionalised PDMS membranes for the pervaporative recovery of organics from aqueous streams. Journal of Membrane Science, 137, 63-88.

3. Car, A., Stropnik, C., Yave, W. & Peinemann, K.-V. 2008a. Pebax®/polyethylene glycol blend thin film composite membranes for CO_2 separation: performance with mixed gases. Separation and Purification Technology, 62, 110-117.

4. Car, A., Stropnik, C., Yave, W. & Peinemann, K.-V. 2008b. PEG modified poly (amide-b-ethylene oxide) membranes for CO_2 separation. Journal of Membrane Science, 307, 88-95.

5. Cheng, J., Hu, L., Ji, C., Zhou, J. & Cen, K. 2015. Porous ceramic hollow fiber-supported Pebax/PEGDME composite membrane for CO_2 separation from biohythane. RSC Advances, 5, 60453-60459.

6. Cheng, J., Hu, L., Li, Y., Ji, C., Zhou, J. & Cen, K. 2016. Improving CO_2 permeability of ceramic hollow fibre-supported composite membranes by blending an ionic liquid in the Pebax/PEGDME selective layer. RSC

Advances, 6, 2055-2064.

7. Choi, S.-H., Tasselli, F., Jansen, J. C., Barbieri, G. & Drioli, E. 2010. Effect of the preparation conditions on the formation of asymmetric poly (vinylidene fluoride) hollow fibre membranes with a dense skin. European Polymer Journal, 46, 1713-1725.

8. Choi, W., Ingole, P. G., Park, J.-S., Lee, D.-W., Kim, J.-H. & Lee, H.-K. 2015. H_2/CO mixture gas separation using composite hollow fiber membranes prepared by interfacial polymerization method. Chemical Engineering Research and Design, 102, 297-306.

9. Freeman, B., Yampolskii, Y. & Pinnau, I. 2006. Materials science of membranes for gas and vapor separation, John Wiley & Sons.

10. Ismail, A. F., Khulbe, K. & Matsuura, T. 2015. Gas Separation Membranes: Polymeric and Inorganic, Springer.

11. Ismail, A. F. & Lai, P. Y. 2003. Effects of phase inversion and rheological factors on formation of defect-free and ultrathin-skinned asymmetric polysulfone membranes for gas separation. Separation and Purification Technology, 33, 127-143.

12. Kargari, A., Shamsabadi, A. A. & Babaheidari, M. B. 2014. Influence of coating conditions on the H 2 separation performance from H_2/CH_4 gas mixtures by the PDMS/PEI composite membrane. International Journal of Hydrogen Energy, 39, 6588-6597.

13. Li, S., Wang, Z., Zhang, C., Wang, M., Yuan, F., Wang, J. & Wang, S. 2013a. Interfacially polymerized thin film composite membranes containing ethylene oxide groups for CO_2 separation. Journal of Membrane Science, 436, 121-131.

14. Li, T., Pan, Y., Peinemann, K.-V. & Lai, Z. 2013b. Carbon dioxide selective mixed matrix composite membrane containing ZIF-7 nano-fillers. Journal of Membrane Science, 425, 235-242.

15. Lillepärg, J., Georgopanos, P., Emmler, T. & Shishatskiy, S. 2016. Effect of the reactive amino and glycidyl ether terminated polyethylene oxide additives on the gas transport properties of Pebax® bulk and thin film composite membranes. RSC Advances. 6, 11763-11772.

16. Liu, L., Chakma, A. & Feng, X. 2004. A novel method of preparing ultrathin poly (ether block amide) membranes. Journal of Membrane Science, 235, 43-52.

17. Madaeni, S., Badieh, M. & Vatanpour, V. 2013. Effect of coating method on gas separation by PDMS/PES membrane. Polymer Engineering & Science, 53, 1878-1885.

18. Matsuura, T. 1993. Synthetic membranes and membrane separation processes, CRC press.

19. Mosleh, S., Mozdianfard, M., Hemmati, M. & Khanbabaei, G. 2017. Mixed matrix membranes of Pebax1657 loaded with iron benzene -1,3,5- tricarboxylate for gas separation. Polymer Composites, 38, 1363-1370.

20. Murali, R. S., Ismail, A. F., Rahman, M. A. & Sridhar, S. 2014. Mixed matrix membranes of Pebax-1657 loaded with 4A zeolite for gaseous separations. Separation and Purification Technology, 129, 1-8.

21. Murali, R. S., Sridhar, S., Sankarshana, T. & Ravikumar, Y. 2010. Gas permeation behavior of Pebax-1657 nanocomposite membrane incorporated with multiwalled carbon nanotubes. Industrial & Engineering Chemistry Research, 49, 6530-6538.

22. Nafisi, V. & Hägg, M.-B. 2014. Development of dual layer of ZIF-8/PEBAX-2533 mixed matrix membrane for CO_2 capture. Journal of Membrane Science, 459, 244-255.

23. Ramon, G. Z., Wong, M. C. & Hoek, E. M. 2012. Transport through composite membrane, part 1: Is there an optimal support

membrane? Journal of Membrane Science, 415, 298-305.

24. Reijerkerk, S. R., Jordana, R., Nijmeijer, K. & Wessling, M. 2011. Highly hydrophilic, rubbery membranes for CO_2 capture and dehydration of flue gas. International Journal of Greenhouse Gas Control, 5, 26-36.

25. Ren, X., Ren, J. & Deng, M. 2012. Poly (amide-6-b-ethylene oxide) membranes for sour gas separation. Separation and Purification Technology, 89, 1-8.

26. Robeson, L. M. 2008. The upper bound revisited. Journal of Membrane Science, 320, 390-400.

27. Scofield, J. M. P., Gurr, P. A., Kim, J., Fu, Q., Kentish, S. E. & Qiao, G. G. 2016. Blends of fluorinated additives with highly selective thin-film composite membranes to increase CO_2 permeability for CO_2/N_2 gas separation applications. Industrial & Engineering Chemistry Research, 55, 8364-8372.

28. Vankelecom, I., Moermans, B., Verschueren, G. & Jacobs, P. 1999. Intrusion of PDMS top layers in porous supports. Journal of Membrane Science, 158, 289-297.

29. Wijenayake, S. N., Panapitiya, N. P., Nguyen, C. N., Huang, Y., Balkus, K. J., Musselman, I. H. & Ferraris, J. P. 2014. Composite membranes with a highly selective polymer skin for hydrogen separation. Separation and Purification Technology, 135, 190-198.

30. Yampolskii, Y. & Freeman, B. 2010. Membrane gas separation, Wiley Online Library.

31. Yong, W. F., Li, F. Y., Xiao, Y. C., Chung, T. S. & Tong, Y. W. 2013. High performance PIM-1/Matrimid hollow fiber membranes for CO_2/CH_4, O_2/N_2 and CO_2/N_2 separation. Journal of Membrane Science, 443, 156-169.

32. Zhu, L., Jia, W., Kattula, M., Ponnuru, K., Furlani, E. P. & Lin, H. 2016. Effect of porous supports on the permeance of thin film composite membranes: Part I. Track-etched polycarbonate supports. Journal of Membrane Science, 514, 684-695.

پیش‌بینی حلالیت گازهای H_2S و CO_2 در محلول‌های MDEA و MDEA/PZ توسط بسته‌های ترمودینامیکی ACID GAS و ELECNRTL

- امید صباغ – میثم وحیدی فردوسی – محمد علی فنائی*

گروه مهندسی شیمی، دانشگاه فردوسی مشهد، مشهد، ایران

(ایمیل نویسنده مسئول: fanaei@um.ac.ir)

چکیـــــــده

در این مطالعه، میزان حلالیت گازهای اسیدی سولفید هیدروژن و دی‌اکسیدکربن در محلول‌های آبی MDEA و MDEA/PZ توسط بسته‌های مختلف ترمودینامیکی مورد ارزیابی قرار گرفته است. مقایسه نتایج مدل‌سازی با مجموعه‌ای از اطلاعات صنعتی و آزمایشگاهی که از سال ۱۹۹۷ تا ۲۰۱۰ منتشر گردیده، نشان از دقت بالای پیش‌بینی حلالیت گازهای اسیدی در محلول‌های مذکور با بسته ترمودینامیکی ACID GAS (نرم‌افزار اسپن هایسیس ۸/۳) در مقایسه با بسته ترمودینامیکی ELECNRTL (نرم‌افزار اسپن پلاس ۸/۲) بویژه در محدوده غلظت‌های عملیاتی واحدهای شیرین سازی گاز طبیعی دارد.

واژگان کلیدی: MDEA، PZ، بسته ترمودینامیکی، حلالیت گازهای اسیدی، ACID GAS، ELECNRTL.

بررسی حلالیت هیدروژن سولفید در گوگرد مذاب با استفاده از روش تیتراسیون برگشتی یدومتری

- فائزه تاری[1]، مرضیه شکرریز[1*]، سعید زرین پاشنه[2]، احمد روزبهانی[1]

۱. پژوهشکده توسعه فناوریهای شیمیایی، پلیمری و پتروشیمیایی، پژوهشکده تحقیق و توسعه صنایع پایین دستی صنعت نفت، پژوهشگاه صنعت نفت ایران، تهران، ایران. کدپستی ۸۹۹۱۵۶۶۴۱

۲. پژوهشکده گاز، پژوهشکده تحقیق و توسعه صنایع پایین دستی صنعت نفت، پژوهشگاه صنعت نفت ایران، تهران، ایران. کدپستی ۸۹۹۱۵۶۶۴۱

(ایمیل نویسنده مسئول: Shekarriz@ripi.ir)

چکیـــــــده

به منظور انجام بررسی های آزمایشگاهی بر روی ترکیب و رفتار گوگرد مذاب حاصل از واحد کلاوس، نیاز است که گوگرد مذاب حاوی ppmw ۲۰۰-۲۵۰ هیدروژن سولفید (H_2S) و هیدروژن پلی سولفید (H_2S_x) حل شده باشد. در این پژوهش تولید این محصول با استفاده از تزریق هیدروژن سولفید به گوگرد مذاب مطالعه شد و نمونه مناسبی جهت بررسی های آزمایشگاهی تولید گردید. محصول گوگرد مذاب حاصل در این روش توسط تزریق هیدروژن سولفید تحت فشار به سطح گوگرد جامد و عملیات حرارتی در طی زمان مناسب ایجاد شده است. همچنین طبق نتایج حاصل از آنالیز یدومتری برگشتی، نمونه گوگرد مذاب نهایی دارای ppmw ۵۰۰-۱۱۰۰ هیدروژن سولفید و هیدروژن پلی سولفید محلول بر اساس میزان فشار تزریقی بوده است.

واژگان کلیدی: گوگرد مذاب، گازدهی، گاززدایی، تیتراسیون برگشتی یدومتری.

آنالیز فرآیند آشام غیر همسو از طریق حل مساله با روش تفاضل محدود و با در نظر گرفتن نیروی گرانش

- مژگان ابراهیمی نژاد حسن آبادی[1]، محمد رضا احسانی[1*]، مهناز طیاری[2]، محمد نیکوکار[3]

۱. دانشکده مهندسی شیمی، دانشگاه صنعتی اصفهان، اصفهان، ایران

۲. دانشکده مهندسی شیمی، دانشگاه تهران، تهران، ایران

۳. پژوهشکده ازدیاد برداشت از مخازن نفت و گاز ، تهران، ایران

(ایمیل نویسنده مسئول: Ehsanimr@cc.iut.ac.ir)

چکیـــــــده

فرآیند آشام خود به خودی غیرهمسو یکی از مهمترین روش های برداشت نفت از مخازن شکاف دار آبدوست با تراوایی پایین بلوک ماتریکس به حساب می آید. این مطالعه بر آن است که از طریق مدلسازی عددی، فرآیند آشام را که در آن آب از طریق نیروی های گرانش و مویینگی نفت موجود در بستر مکعبی شکل را جاروب می کند را بررسی کند و اثر نیروی گرانش بر عملکرد این فرآیند را معین کند. در این تحقیق، پدیده ی آشام به عنوان فرآیند نفوذی در نظر گرفته شده است. روش عددی تفاضل محدود ضمنی برای حل معادلات حاکم بر فرآیند آشام خودبه خودی به کار گرفته شده است. دقت مدل ارائه شده با صحه سنجی و مقایسه خروجی این مدل ریاضی و داده های آزمایشگاهی بررسی شده است.

واژگان کلیدی: آشام خود به خودی، آشام غیرهمسو، برداشت نفت، نیروی گرانش.

تاثیر عملکرد کمپرسور بر ظرفیت جریان خطوط انتقال گاز

• سید محمد فاطمی[1]، مرتضی اسفندیاری[2*]، مهدی کولیوند سالوکی[3]

۱. ستاد مهندسی نفت، شرکت ملی نفتخیز جنوب ، اهواز، ایران

۲. گروه مهندسی شیمی، دانشگاه بجنورد، بجنورد، ایران

۳. پژوهشکده گاز، پژوهشگاه صنعت نفت، تهران ، ایران

(ایمیل نویسنده مسئول: M.Esfandyari@ub.ac.ir)

چکیـــــــده

ظرفیت جریان گاز خط انتقال گاز معمولا تحت تأثیر پارامترهای مختلف قرار می گیرد. در این مطالعه چند عامل تعیین کننده برای تحلیل حساسیت پیش بینی ظرفیت جریان در IGAT-IV انتخاب شده اند. این پارامترها شامل پارامترهای خط لوله، پارامترهای گاز، پارامترهای سیستم، پارامترهای انتقال حرارت، پارامترهای متراکم پذیری و پارامترهای مصرف سوخت کمپرسور می باشند. محاسبات مورد نیاز با توسعه برنامه نویسی توسط Microsoft Visual Basic به صورت دقیق انجام شده است. علاوه بر این، یک برنامه کامپیوتری توسط MATLAB برای بدست آوردن منحنی های عملکرد کمپرسور نوشته شده است. این منحنی برای طراحی و بهینه سازی ایستگاه های کمپرسور مورد استفاده قرار گرفته است. از تحقیقات حاضر، معادله های کاملاً آشفته AGA ، Colebrook-White و Weymouth جریان خطوط انتقال را به خوبی پیش بینی می نماید.۸۷/۷۵ درصد تغییرات جریان به دلیل ۱ درصد تغییرات ایزونتروپیک است که تاثیر بسیار زیادی بر ظرفیت جریان دارد و همچنین ۱۰ تا ۳۰ درصد تغییرات جریان ناشی از ۱ درصد ضریب تراکم پذیری مکش و تخلیه می باشد. در نهایت ۱ تا ۱۰ درصد تغییرات جریان به دلیل ۱ درصد تغییرات اسب بخار کمپرسور، دمای مکش و تخلیه کمپرسور و تغییرات بازده آدیاباتیک می باشد که آنها تاثیر متوسط بر ظرفیت جریان دارند. و پارامترهای دیگر تاثیر قابل توجهی بر ظرفیت جریان ندارند.

واژگان کلیدی: خطوط لوله انتقال گاز، ظرفیت جریان، پارامترهای تراکم پذیری، پارامترهای مصرف سوخت کمپرسور.

افت فشار برج جذب آکنده نامنظم در رژیم جریان گذرا

- سیده گیتا شرفی، رهبر رحیمی* ، مرتضی زیودار

۱. گروه مهندسی شیمی، دانشگاه سیستان و بلوچستان، زاهدان، ایران

(ایمیل نویسنده مسئول: rahimi@hamoon.usb.ac.ir)

چکیـــــــده

در این پژوهش از روش دینامیک سیالات محاسباتی برای توصیف جریان در بستر آکنده برج جذب با آکنه های نامنظم پرداخته شده است. در این بررسی برجی در مقیاس نیمه صنعتی با آکنه های راشیگ ۱ سانتیمتری بوسیله دینامیک سیالات محاسباتی مورد شبیه سازی در مقیاس ماکرو قرار گرفته است. ارتفاع برج در حدود ۱۷۵ سانتیمتر است. محدوده سرعت هوا ۱/۵ الی ۵ متربرثانیه و افت فشار اندازه گیری شده ۱/۵ الی ۱۲ پاسکال بر واحد متر است. پدیده اثر دیواره که منجر به توزیع تخلخل شعاعی در ناحیه آکنده میشود با دیدگاه کلرک بیان شده است. تعریف توزیع تخلخل شعاعی کلرک در مدل CFD در پیش بینی افت فشار حاصل از محیط آکنده با آکنه های راشیگ موفق بوده است.پیش بینی افت فشار خشک توسط مدل تنها در حدود ۴٪ با نتایج آزمایشگاهی اختلاف دارد. دیدگاه پیش بینی افت فشار ارگان، در دو حالت بررسی با تخلخل متوسط و توزیع تخلخل شعاعی، با دیدگاه رایکلت مورد مقایسه قرار گرفته است. در این بررسی دیدگاه پیش بینی افت فشار براساس رابطه ارگان در هر دو روش به نسبت دیدگاه رایکلت در پیش بینی داده های آزمایشگاهی دقیق تر بوده و تنها ۶٪ از نتایج آزمایشگاهی اختلاف داشت.

واژگان کلیدی: افت فشار، برج جذب آکنده ، آکنه نامنظم، دینامیک سیالات محاسباتی

اثر روش پوشش و فشار و دمای خوراک بر عملکرد جداسازی دی‌اکسیدکربن/متان غشاهای مرکب Pebax/PES

- حمیدرضا افشون[۱]، مهدی پورافشاری چنار[۱*]، احمد فوزی اسماعیل[۲]

۱. گروه مهندسی شیمی، دانشکده مهندسی، دانشگاه فردوسی مشهد، مشهد، ایران

۲. مرکز تحقیقات پیشرفته فناوری غشا (AMTEC)، دانشگاه فناوری مالزی (UTM)، مالزی

(ایمیل نویسنده مسئول: pourafshari@um.ac.ir)

چکیـــــــده

در این مطالعه غشای مرکب Pebax/PES با پوشش تک لایه Pebax-1657 بر روی لایه متخلخل PES ساخته شد. روش‌های ریخته‌گری و ریزش محلول برای پوشش لایه بالایی استفاده شدند. تاثیر روش پوشش و شرایطی مانند غلظت محلول Pebax و دما بر تراوش‌پذیری CO_2 و CH_4 غشاهای مرکب ساخته شده بررسی شد. تصاویر SEM برای بررسی ساختار غشاهای ساخته شده استفاده شد. گازهای خالص CO_2 و CH_4 برای بررسی خواص تراوش‌پذیری غشاهای ساخته شده در فشار و دمای خوراک به ترتیب ۱ تا ۱۲ barg و ۵۲ تا ۵۵ °C استفاده شدند. نتایج به‌دست آمده نشان داد که زیرلایه PES قبل از پوشش هیچ گزینش‌پذیری CO_2/CH_4 نداشته است. نتایج همچنین نشان داد که غشاهای ساخته شده با روش ریزش محلول گزینش‌پذیری CO_2/CH_4 بالاتری نسبت به غشاهای ساخته شده با روش ریخته‌گری داشته که این به دلیل شکل‌گیری لایه انتخابگر بدون نقص در حین پوشش با روش ریزش محلول است. تراوایی دی‌اکسیدکربن و متان با افزایش دمای خوراک از ۲۵ تا ۵۵ °C افزایش یافت. نتایج همچنین نشان داد که با افزایش فشار خوراک از ۲ تا ۱۲ barg تراوایی CO_2 از ۶/۸ تا ۱/۱۰ GPU افزایش داشته، ضمن این‌که تراوایی متان تقریبا ثابت مانده و در نتیجه گزینش‌پذیری CO_2/CH_4 از ۲۷ به ۴۲ افزایش داشته است.

واژگان کلیدی: **Pebax**، غشای مرکب، جداسازی **CO_2**، روش پوشش، فشار خوراک، دما

Journal of Gas Technology • Volume 3 • January 2018

ISSN: 2588-5596